

Research & Reviews: Journal of Material Sciences

Advances in Photo-catalytic Materials for Environmental Applications

Elsalamony RA*

Egyptian Petroleum Research Institute, Cairo, Egypt

Research Article

Received date: 04/04/2016

Accepted date: 17/05/2016

Published date: 27/05/2016

*For Correspondence

Elsalamony RA, Egyptian petroleum research institute, Cairo, Egypt, Tel: 00201010707023

Email: radwa2005@hotmail.com

Keywords: Photodegradation; Dyes; Doping TiO₂; Metal and non-metal doping.

ABSTRACT

The growth of industry worldwide has extremely increased the generation and accumulation of waste by products. This has caused severe environmental problems that have become a major concern. Because of this, photo-catalytic pollutant degradation provided great opportunities and challenges in the field of environmental science. TiO₂ nanoparticles have been extensively investigated for photo-catalytic decomposition of organic compounds. TiO₂ is considered close to an ideal semiconductor for photo-catalysis but possesses certain limitations such as poor absorption of visible radiation and rapid recombination of photo generated electron/hole pairs. In this review article, various methods used to enhance the photo-catalytic characteristics of TiO₂ including self-doping TiO₂, doping TiO₂ with metal and non-metal. Improving catalytic efficiency and exploring the reaction mechanism of photo-catalytic degradation of dyes as a model organic compound.

INTRODUCTION

Over two thirds of Earth's surface is covered by water; less than a third is taken up by land. As Earth's population continues to grow, people are putting ever-increasing pressure on the planet's water resources. In a sense, our oceans, rivers, and other inland waters are being "squeezed" by human activities—not so they take up less room, but so their quality is reduced. Poorer water quality means water pollution. We know that pollution is a human problem because it is a relatively recent development in the planet's history: before the 19th century Industrial Revolution, people lived more in harmony with their immediate environment. As industrialization has spread around the globe, so the problem of pollution has spread with it. When Earth's population was much smaller, no one believed pollution would ever present a serious problem. It was once popularly believed that the oceans were far too big to pollute. Today, with around 7 billion people on the planet, it has become apparent that there are limits. Pollution is one of the signs that humans have exceeded those limits.

Water pollution can be defined in many ways. Usually, it means one or more substances have built up in water to such an extent that they cause problems for animals or people. Water pollution almost always means that some damage has been done to an ocean, river, lake, or other water source. A 1969 United Nations report defined ocean pollution as: "The introduction by man, directly or indirectly, of substances or energy into the marine environment (including estuaries) resulting in such deleterious effects as harm to living resources, hazards to human health, hindrance to marine activities, including fishing, impairment of quality for use of sea water and reduction of amenities."

Most water pollution doesn't begin in the water itself. Take the oceans: around 80 percent of ocean pollution enters our seas from the land. Virtually any human activity can have an effect on the quality of our water environment. When farmers fertilize the fields, the chemicals they use are gradually washed by rain into the groundwater or surface waters nearby. Sometimes the causes of water pollution are quite surprising. Chemicals released by smokestacks (chimneys) can enter the atmosphere and then fall back to earth as rain, entering seas, rivers, and lakes and causing water pollution. That's called atmospheric deposition. Water pollution has many different causes like: Sewage, Nutrients, Chemical waste, radioactive waste, Oil pollution, Plastics and Alien species. The common pollutants include toxic organic compounds like chlorinated and non-chlorinated aliphatic and aromatic compounds, dyes, inorganic compounds like heavy metals, noxious gases like NO_x, SO_x, CO and NH₃, and pathogens like bacteria, fungi and viruses.

Advanced Oxidation Processes

However; the research community aims to develop clean and green processes to degrade the pollutants before they are admitted into the atmosphere and water bodies. Photo-catalysis has become an integral part of the Advanced Oxidation Processes (AOPs), refers to a set of chemical treatment procedures designed to remove organic (and sometimes inorganic) materials in water and waste water by oxidation through reactions with hydroxyl radicals ($\cdot\text{OH}$)^[1]. In real-world applications of wastewater treatment, however, this term usually refers more specifically to a subset of such chemical processes that employ ozone (O_3), hydrogen peroxide (H_2O_2) and/or UV light^[2]. One such type of process is called in situ chemical oxidation. AOPs rely on in-situ production of highly reactive hydroxyl radicals ($\cdot\text{OH}$). These reactive species are the strongest oxidants that can be applied in water and can virtually oxidize any compound present in the water matrix, often at a diffusion controlled reaction speed. Consequently, $\cdot\text{OH}$ reacts unselectively once formed and contaminants will be quickly and efficiently fragmented and converted into small inorganic molecules. Hydroxyl radicals are produced with the help of one or more primary oxidants (e.g. ozone, hydrogen peroxide, oxygen) and/or energy sources (e.g. ultraviolet light) or catalysts (e.g. titanium dioxide). Precise, pre-programmed dosages, sequences and combinations of these reagents are applied in order to obtain a maximum $\cdot\text{OH}$ yield. In general, when applied in properly tuned conditions, AOPs can reduce the concentration of contaminants from several hundred ppm to less than 5 ppb and therefore significantly bring COD and TOC down, which earned it the credit of –water treatment processes of the 21st century^[3].

The AOP procedure is particularly useful for cleaning biologically toxic or non-degradable materials such as aromatics, pesticides, petroleum constituents, and volatile organic compounds in waste water^[4]. Additionally, AOPs can be used to treat effluent of secondary treated wastewater which is then called tertiary treatment^[5]. The contaminant materials are converted to a large extent into stable inorganic compounds such as water, carbon dioxide and salts, i.e. they undergo mineralization. A goal of the waste water purification by means of AOP procedures is the reduction of the chemical contaminants and the toxicity to such an extent that the cleaned waste water may be reintroduced into receiving streams or, at least, into a conventional sewage treatment. Recently, Ultrasound (US), microwave radiation and electrolysis are being coupled to the above AOPs in order to further enhance the decomposition of the pollutants.

Photo-catalysis has found several applications in the field of environment: destruction of aqueous pollutants^[6], air purification, metal recovery, and especially more recently, production of materials such as self-cleaning glass surfaces^[7]. Applications for photo-catalytic decontamination of water have already arrived at the stage of pilot plant. Reactors are artificial radiation source on the market. Despite the small percentage of the absorbed solar radiation (3.5%) by TiO_2 solar processes have been developed^[8].

Definition of Photo-Catalysis

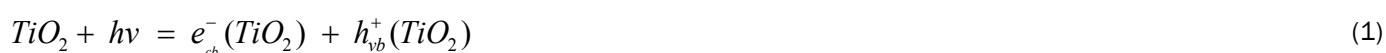
The catalyst is in the heart of the photo-catalytic process. Since photo-catalysis is based on the excitation of a photocatalyst with irradiation of light energy at least equal to that of the Band Gap Energy (BE). These photocatalyst are more commonly called semiconductors. There are many semiconductor metal oxides used for photo-catalytic properties namely: TiO_2 , ZnO, ZnS, WO_3 , CdS, SnO_2 , GaP etc.

Among the list of semiconductors reported in the literature, TiO_2 has proven most suitable for most common environmental applications. Because it is biologically and chemically inert, resistant to chemical corrosion and can work at ambient temperature and pressure, without addition of chemical species, low toxicity, low cost, and abundance as raw material. TiO_2 an important material in many practical applications, and, in commercial products ranging from drugs to foods, cosmetics to catalysts, paints to pharmaceuticals, and sunscreens to solar cells in which TiO_2 is used as a desiccant, brightener, or reactive mediator^[9].

Titanium dioxide or titania (TiO_2) was first produced commercially in 1923. It is obtained from a variety of ores. TiO_2 is a typical n-type semiconductor. It possesses three crystal polymorphs in nature: brookite, anatase, and rutile^[10]. Brookite is rare in nature, uncommon, unstable and hence does not feature in discussion of catalyst materials. Among them, the TiO_2 exists mostly as rutile and anatase phases which both of them have the tetragonal structures. However, rutile is a high-temperature stable phase and has an optical energy band gap of 3.0 eV (415 nm), anatase is formed at a lower temperature with an optical energy band gap of 3.2 eV (380 nm). Additionally, TEM was used to further examine the crystallite/particle size, the crystallinity and morphology of samples. TiO_2 powders in rutile phase consist of both spherical and cubic shape; on the contrary, the particle of TiO_2 in anatase phase has mostly spherical morphology^[11]. In this review, we will first describe the mechanism of UV photo-catalysis, and the synthesis of nano- TiO_2 by sol-gel technique. We then discuss the different doping methods of inducing the visible light response of TiO_2 . Finally; the photo-catalytic degradation mechanism of dyes as water contaminants are discussed.

Mechanism of Photo-Catalysis

The principle of photo-catalysis is based on the excitation of a semiconductor (usually titanium dioxide TiO_2) by light (UV or visible). Under the action of photons, the semiconductor (or catalyst) produces highly oxidizing free radicals allowing the destruction of compounds adsorbed on its surface. This produces electron-hole (e^-/h^+) pairs as in Equation (1) (**Figure 1**):



The semiconductor TiO_2 converts photon energy into chemical energy by oxidation-reduction reaction; where cb is the

conduction band and v_b is the valence band. Thus, as a result of irradiation, the TiO_2 particle can behave either as an electron donor or acceptor for molecules in contact with the semiconductor. The electron and hole can recombine, releasing the absorbed light energy as heat, with no chemical reaction taking place. On the other hand, they can participate in redox reactions with adsorbed species as the valence band hole is strongly oxidizing while the conduction band electron is strongly reducing. On the semiconductor surface, the excited electron and the hole can participate in redox reactions with water, hydroxide ion (OH^-), organic compounds or oxygen leading to mineralization of the pollutant.

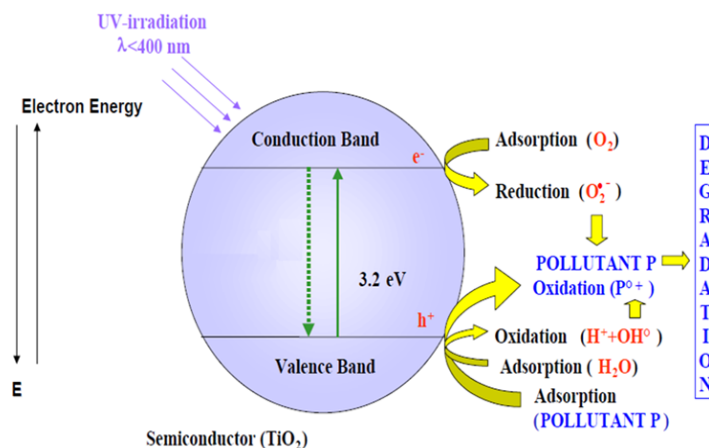


Figure 1. General mechanism of photo-catalysis.

In fact, research shows that the charges can react directly with adsorbed pollutants, but reactions with water are predominant since the water molecules are more abundant than contaminant molecules. Consequently, oxidation of water or OH^- by the hole produces the hydroxyl radical ($\cdot OH$), a powerful oxidant. An important reaction of the conduction band electron is reduction of adsorbed oxygen to oxygen radicals and this prevents the electron from recombining with the hole and results in an accumulation of oxygen radicals that can also participate in degrading contaminants in solution^[12,13]. A mechanism involving radical reactive species, through the following series reactions Equations (2 - 6):



Published work indicate that heterogeneous photo-catalytic process involves at least five separate reaction steps^[14] and include (1) diffusion of reactants to the surface of semiconductor, (2) adsorption of reactants onto the surface of semiconductor, (3) reaction on the surface of semiconductor, (4) desorption of products from the surface of the semiconductor and (5) diffusion of products from the surface of the semiconductor. There are two routes through which OH radicals can be formed—the reaction of the valence-band holes with either adsorbed H_2O or with the surface OH groups on the TiO_2 particle. These processes have been summarized using appropriate equations^[15].

PREPARATION METHODS OF TiO_2 NANO-PARTICLES

For photo-catalytic applications, nano-sized TiO_2 is preferred compared to bigger sized TiO_2 particles. The two most important properties of a nano material, which makes it superior to other microscopic or macroscopic particles for applications in catalysis, are (i) the high surface to volume ratio, and (ii) the quantum confinement at the nano scale. The first property results in catalysts with high surface area and high porosity, which ensures enhanced reaction rates due to the high level of interaction of the reactants with the active sites. The second property governs the transport of electrons and holes from the bulk to the surface of the material, whose length scale is also of the order of a few nanometers (called as electron Bohr radius). Moreover, for photo-applications, the catalyst should absorb, and not block or scatter, incident radiation, and generate charge carriers by band gap excitation. This is possible only with nano-sized semiconductor materials with suitable band gap energy. Therefore, owing to the enhanced molecular transport properties at the surface, it is evident that nano-sized materials are beneficial as photocatalysts. Nano- TiO_2 photocatalysts have been synthesized in different shapes and morphologies, which include, nanoparticles, nanotubes^[16], nanopillars and nanowire arrays^[17], nanorods^[18], mesoporous structures^[19] nanobowls, nanowhiskers, aerogels, nanosheets, opal and inversed opals^[20,21].

The synthesis routes can be broadly classified as solution phase and gas phase techniques. Solution phase synthesis is

the most preferred technique for the preparation of TiO_2 in the form of powders and thin films. Chemical precipitation method^[22], Chemical Vapour Deposition (CVD)^[23], the sol-gel technique^[24], sputtering^[25], hydrolysis, micro-emulsion method^[26], spray deposition^[27], aerosol-assisted chemical vapour deposition^[28], thermal plasma^[29], hydrothermal method^[30], microwave assisted hydrothermal synthesis^[31], solvothermal method^[32] and flame combustion method^[33] electrodeposition^[33], sonochemical method^[34], and microwave method^[35].

Each of the above synthesis methods possesses a unique advantage over the other techniques and the characteristics of the final product vary from one method to another. The TiO_2 nanoparticles like the phase composition (anatase : rutile), particle size, porosity, surface area, band gap and surface hydroxyl content can be tailored by varying the reaction conditions like: the precursor compound (TiCl_4 , titanium(IV) isopropoxide, etc.), hydrolyzing agent (in the case of sol-gel synthesis), fuel (in the case of solution combustion synthesis), molar composition of the reactants, reaction temperature, reaction time (ageing time), calcination temperature and presence of gas atmosphere (air, Ar, NH_3). Among these methods sol-gel method is a simple method to synthesis TiO_2 nanoparticles.

Sol-Gel Method

It is a versatile process used in making various ceramic materials. The sol-gel technique has been reviewed by a number of investigators^[36,37].

In sol-gel chemistry, nanometer-sized particles form and then connect with one another to create a three-dimensional (3D) solid network. This technique allows scientists to change the composition and structure of materials on the nanometer (billionth-of-a-meter) scale. In addition, this process can be modified to produce sol-gel materials in different forms, such as powders, films, fibers, and freestanding pieces of material called monoliths. For example, a gel can be dried in a sol-gel process to make aerogels, a special class of ultralow-density materials. The sol-gel approach is a cheap and low-temperature technique finely controls the product's chemical composition. Even small quantities of dopants, such as organic dyes and rare earth elements, can be introduced in the sol and end up uniformly dispersed in the final product. The inherent advantages of the sol-gel process are^[38]:

1. Better homogeneity from raw materials.
2. Better purity from raw materials.
3. Lower temperature of preparation.
4. Good mixing for multi-component systems.
5. Effective control of particle size, shape, and properties.
6. Better products from the special properties of the gel.
7. The creation of special products such as films.
8. The creation of new non-crystalline solids outside the range of normal glass formation.
9. The possibility of designing the material structure and property through the proper selection of sol-gel precursor and other building blocks.

Sol-gel derived materials have diverse applications in optics, electronics, energy, space, bio-sensors, medicine (e.g., controlled drug release), and in reactive material and separation (e.g., chromatography) technology^[39,40].

Procedure of Sol-Gel Method

In a typical sol-gel process, a colloidal suspension, or a sol, is formed from the hydrolysis and polymerization reactions of the precursors, which are usually inorganic metal salts or metal organic compounds such as metal alkoxides. Complete polymerization and loss of solvent leads to the transition from the liquid sol into a solid gel phase. The precursor sol can be either deposited on a substrate to form a film, casted into a suitable container with the desired shape (e.g., to obtain monolithic ceramics, glasses, fibers, membranes, and aerogels), or used to synthesize powders (e.g., microspheres, nanospheres).

Thin films can be produced on a piece of substrate by spin-coating or dip-coating. A wet gel will form when the sol is cast into a mold, and the wet gel is converted into a dense ceramic with further drying and heat treatment. A highly porous and extremely low density material called an aerogel is obtained if the solvent in a wet gel is removed under a supercritical condition.

Ceramic fibers can be drawn from the sol when the viscosity of a sol is adjusted into a proper viscosity range. Ultrafine and uniform ceramic powders are formed by precipitation, spray pyrolysis, or emulsion techniques. Under proper conditions, nanomaterials can be obtained.

Nanostructured TiO_2 has been synthesized with the sol-gel method from hydrolysis of a titanium precursor. This process normally proceeds via an acid-catalyzed hydrolysis step of titanium (IV) alkoxide followed by condensation. The development of Ti-O-Ti chains is favored with low content of water, low hydrolysis rates, and excess titanium alkoxide in the reaction mixture. Three dimensional polymeric skeletons with close packing result from the development of Ti-O-Ti chains. The formation of $\text{Ti}(\text{OH})_4$

is favored with high hydrolysis rates for a medium amount of water. The presence of a large quantity of Ti-OH and insufficient development of three-dimensional polymeric skeletons lead to loosely packed first order particles. Polymeric Ti-O-Ti chains are developed in the presence of a large excess of water. Closely packed first order particles are yielded via a three-dimensionally developed gel skeleton. **Figure 2** summarized procedures for preparation of nanoparticles by sol-gel method.

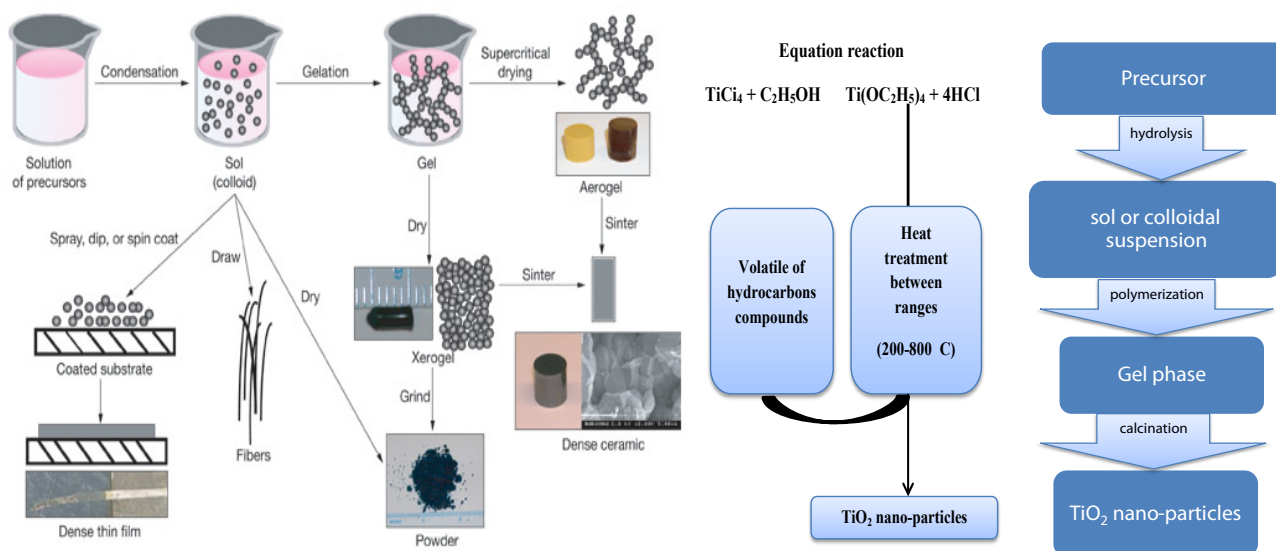


Figure 2. Summarized procedures for preparation of nanoparticles by sol-gel method.

In general; this method based on the mixing, polymerizing, hydrolysis, aging and calcination of various titanium molecular precursors in aqueous solutions or an organic solvent [41-46]. All these factors with new condition can be used for making and controlling the diameter of nanoparticles [47,48]. In view of the synthetic methods there is no letter, known to us, which is used amount of solvent and precursor, mixing method, gelatinizing time, PH control, aging, using ultrasound waves [49] and calcination temperature for synthesis and controlling of diameter of TiO₂ nanoparticles.

In comparison to other phases, using anatase phase of TiO₂ nanoparticles with controlled diameters, the high homogeneity, good morphology, high surface area and porosity is very suitable to photocatalytic applications because of higher electron mobility, lower fixed dielectric and density [50-52]. However, thermodynamic stability is particle-size dependent and at particle diameters below 15 nm, anatase is more stable than rutile [53].

Anatase TiO₂ nanoparticles was successfully synthesized by the sol-gel method using TiCl₄ as a precursor and just ethanol solution [54]. The size of anatase TiO₂ nanoparticles could be promoted by decreasing the gelatinizing time and using ultrasound waves. The diameter of anatase TiO₂ nanoparticles increased with increasing calcination temperature and/or gelatinization time; moreover the crystallinity, homogeneity and morphology of TiO₂ nanoparticles become better. Independent changes of calcination temperature and/or gelatinization time accompanied by ultrasonic waves and specific PH value could alter diameter of the TiO₂ nanoparticles. The results appeared that the excellent TiO₂ nanoparticles exhibited 500 °C annealing temperature and 1/2 volumetric percentage of precursors [55]. Sol gel is the excellent method to synthesis of TiO₂ nanoparticles semiconductor, increasing of efficiency of photo-catalytic degradation for pollutions due to increase in surface area and decreasing in particle size distribution and also the generation of nanoparticles lead to a high-throughput and cost-effective procedures.

Venkatachalam et al. [56] prepared TiO₂ by sol-gel method using titanium (IV) isopropoxide. Effect of hydrolyzing agent, reactant molar ratio, aging temperature, aging time and calcinations temperature were studied; maximum surface area=125 m² g⁻¹; min. crystallite size=6 nm; band gap=3.2±0.1 eV; mixture of anatase and rutile phase was obtained. Highly crystalline anatase TiO₂ nanoparticles with different sizes and shapes could be obtained with the polycondensation of titanium alkoxide in the presence of tetramethyl ammonium hydroxide [57,58]. **Figure 3** shows the TEM images of TiO₂ nanoparticles prepared by sol-gel method.

Alternative Method for Synthesis TiO₂

The sol-gel method requires an acid or base catalyst in order to drive hydrolysis and poly-condensation processes. TiO₂ nanoparticles in acid or base solution are then obtained after calcination at high temperature. Therefore, the acid or base nature of TiO₂ sol and high temperature calcination limit its application, including the choice of substrates [58-60]. Use of Peroxo Titanic Acid (PTA) is an alternative method for synthesis of pure anatase TiO₂ under neutral pH and low temperature conditions. This method was also reported as an environmental friendly method for synthesis of TiO₂ because peroxotitanium complex molecules can be converted to TiO₂ nanoparticles at relatively low temperature (100 °C) [61]. It was already observed that the photo-catalytic activity of TiO₂ depends on its crystalline structure, crystal size, and surface area. Titanium tetrachloride (TiCl₄) was applied to synthesize peroxotitanium solution and it was noted that TiO₂ nanopowder with a high surface area can be obtained after heating

at 80 °C [62]. Nanoparticles with single anatase phase can be obtained from alkoxide precursor even near room temperature if synthesis conditions are appropriately controlled [63]. The crystalline sizes of PTA-derived anatase from titanium alkoxide precursor are correspondingly smaller than that from TiCl₄ precursor with a same calcination temperature. While the surface of TiCl₄ derived titania is easily attached by large amounts of NH₄⁺ species, no impurity such as organic species and fewer amounts of –O–O– species are detected on the surface of alkoxide derived anatase. Alkoxide-derived anatase has a bimodal pore system inside the mesoporous range with a greater value of specific surface area or pore volume as compared to the TiCl₄ derived anatase. TiO₂ nanoparticles from titanium alkoxide precursor display a much better photo-catalytic activity in comparison with those from TiCl₄ precursor, owing to their smaller crystalline sizes, better porosities, and preferable surface properties.

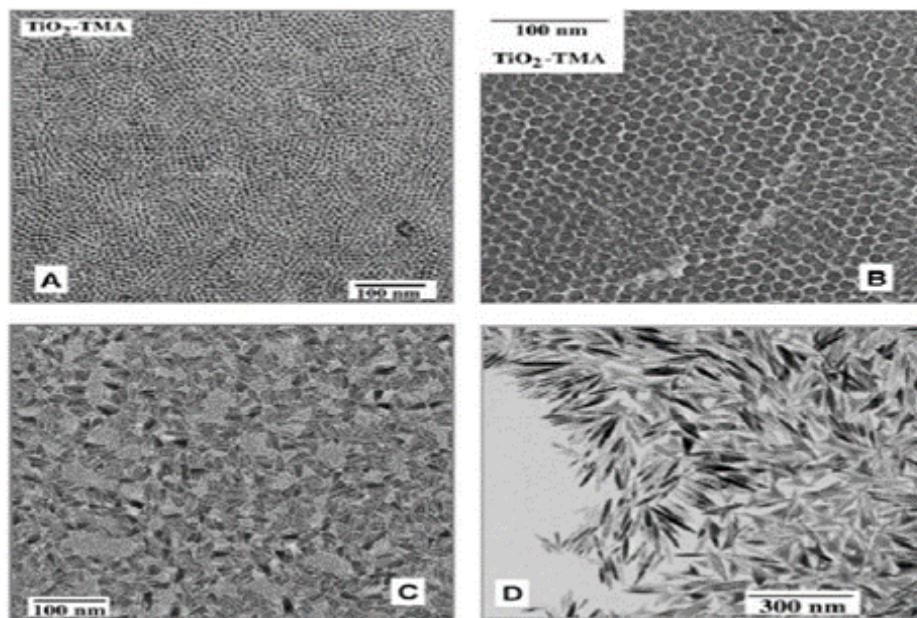


Figure 3. TEM images of TiO₂ nanoparticles prepared by hydrolysis of Ti(OR)₄ in the presence of tetramethylammonium hydroxide [57].

A non-hydrolytic sol-gel process has been employed for the preparation of TiO₂ NPs [64–67]. Titanium tetrahalides, typically titanium tetrachloride (TiCl₄), have been utilized in this process. TiCl₄ was reacted with an oxygen donor, such as diisopropylether, or a titanium alkoxide, typically titanium tetraisopropoxide [68,69]. Since these reactions were conducted in organic solvents without the presence of H₂O (which can also act as an oxygen donor), one of the advantages of this non-hydrolytic sol-gel process is the ability to control the amount of oxygen in the entire process, and this kind of control is extremely attractive for the size control of TiO₂ NPs [64,66]. The first application of Urea-hydrogen peroxide (UHP; CO(NH₂)₂·H₂O₂) for metal oxide preparation reported by UHP can possibly play multiple roles, as an oxidation reagent as well as a donor of water which can cause hydrolysis, and urea which can coordinate to Lewis acid sites. Spheroid anatase TiO₂ NPs have been successfully prepared from TiCl₄ using Urea Hydrogen Peroxide (UHP) as an oxygen donor through a reaction at 80 °C for 30–70 h. The anatase TiO₂ NPs exhibited high dispersibility in water, probably due to the presence of urea. The formation of Cl₂ as well as a comparison with the results of control experiments performed without UHP suggests that anatase TiO₂ NPs were formed via direct oxidation by UHP.

The uniformity of nanoparticles is of remarkable importance because the materials properties are generally directly related to particular characteristics such as size and shape [70,71]. In addition, uniform nanoparticles are potentially required in the area of nanotoxicology to study the effect of nanoparticle size. Thus, a controllable and simple methodology to design monodisperse titania nanoparticles can lead to highly efficient performing materials. Recently, a great deal of research efforts have been devoted to the preparation of monodisperse TiO₂ particles. Eiden-Assmann et al. [72] discussed that particle size and distribution could be controlled by the ionic strength. It has indeed been reported to be directly related to the concentration of salt. These authors prepared monodisperse TiO₂ particles (4200 nm in diameter) using nitrates, KCl, NaCl, CsCl, and LiCl solutions under an inert atmosphere. Han et al. [73] reported an efficient, environmentally friendly and facile sol-gel approach for the controllable synthesis of monodisperse and highly uniform TiO₂ nanoparticles of various sizes in the 10–300 nm range employing different concentrations of a CaCl₂ solution. The prepared TiO₂ nanoparticles were calcined at 500 °C for 1 h to yield nanocrystalline anatase TiO₂. To obtain monodisperse nanoparticles by the sol-gel method, a careful control of nucleation and nanoparticle growth is necessary. The concentration of CaCl₂ solution could be effectively varied as a critical parameter in the preparation of various nanomaterials. Light scattering measurements of these experiments pointed out that Titania nanoparticles as small as 8–10 nm could be synthesized (**Figure 4**).

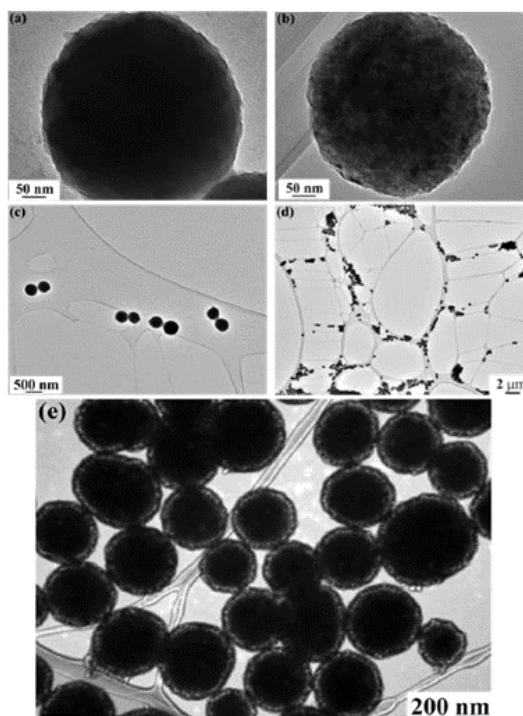


Figure 4. TEM micrographs of monodisperse titania nanoparticles of different sizes before (a, c) and after calcination (b, d, e).

IMPROVING PHOTO-ACTIVITY OF TiO₂

As any semiconductor, TiO₂ is characterized by a band structure in which the energy levels of the valence band (highest occupied level) and conduction band (lowest unoccupied level) are separated by a band gap (E_g) of ca.3.2 eV in the case of anatase^[74]. A photo-catalytic event is initiated when the catalyst is activated by light with an energy content that is sufficient to overcome the band gap^[75]. The incident light wavelength is related to its energy content according to Eq. (8).

$$E = h\nu = \frac{hc}{\lambda} \quad (8)$$

with E , energy content; h , Planck's constant (6.63×10^{-34} Js); ν , frequency of incident light; c , speed of light (3×10^8 ms⁻¹); λ , incident light wavelength. In the case of TiO₂ anatase the band gap energy corresponds to UV light with a wavelength of 388 nm or shorter to bridge the band gap. This enlightens one of the biggest limitations of TiO₂ photo-catalysis, as UV light only contributes to ca.5% of the entire solar spectrum. It would therefore be of tremendous interest to extend the photo-catalytic activity toward the visible light region (400–700 nm) that contributes to an approximate additional 40% of the spectrum^[76].

A lot of effort has been devoted to improve the photo-electronic properties of TiO₂ in order to circumvent one of the two major limitations of TiO₂ photo-catalysis

- i) Tendency for photo generated charge carriers to recombine
- ii) Photoactivity window restricted to UV illumination

Therefore, starting one decade ago, efforts have been devoted to extending the spectral response of pure TiO₂ material (mainly anatase TiO₂) to visible light. These efforts have self-doping TiO₂, doping TiO₂ with non-metal atoms (anion doping) and metal (cation) doping. Co-doping with several elements simultaneously is a variation on the same theme.

Doping

Usually doping involves the use of metals or non-metals and is designed to extend the photo-catalytic activity of a semiconductor lower energy excitation. Technically, doping is the introduction of foreign elements into the parent photocatalyst without giving rise to a new crystallographic forms, phases or structures and the aims are to enhance the net separation of photogenerated charges and thereby efficiently harness the wide visible-light component of about 43% in the solar spectrum as opposed to the narrow ultraviolet component of 5%. It is thus an area of increasing research activity in photo-catalysis.

Self-doping: The term –self-doping refers to the fact that the TiO₂ semi-conductor is changed without the introduction of other metals or non-metals. It is achieved by disrupting the stoichiometric oxygen balance by generating vacancies in the lattice, giving rise to Ti³⁺ sites^[77]. Oxygen vacancies are indeed known to be good e⁻ traps. These trapping states are located just below the conduction band. After visible light absorption they are promoted to the surface where they can participate in surface reactions, which have for instance been employed in the gas phase photo-catalytic oxidation of NO^[78,79]. Mul's group reported the one-step

synthesis of blue colored, Ti^{3+} -rich TiO_2 that is active under visible light illumination^[80], but such materials can suffer from stability issues. On the other hand, Pillai's group recently described the visible light activity of oxygen rich TiO_2 . This was attributed to an upward shift of the valence band after thermal decomposition of peroxo- TiO_2 complexes^[81]. The material remained stable up to 900 °C due to an increased Ti-O- Ti bond strength.

Metal (cation) doping: It is easier to replace Ti^{4+} in TiO_2 with a cation than to substitute O^{2-} with another anion because of the difference in the charge states and ionic radii^[82]. Nano-materials show a higher tolerance to structural distortion than bulk materials due to their inherent lattice strain. As a result, the surface modification of TiO_2 nanoparticles appears to be more beneficial than the modification of bulk TiO_2 ^[83]. Modify pure photo-catalyst materials with metal ions, especially *d*-block metal ions such as Fe^{3+} and Cr^{3+} results in the insertion of impurity energy levels between the parent conduction and valence bands. In this case, the inserted energy levels provide sub-bandgap irradiation from which electrons can be excited from dopant *d*-band to conduction band or from valence band to dopant *d*-band by lower energy photons than are required by the pure photo-catalysts (Figure 5). The resulting energy levels of the dopant states and resulting photo-catalytic activity strongly depend on several factors: the chemical nature of the dopant, its concentration and its chemical and structural environment. It is obvious that every metal will exhibit a different effect on the activity and even for a given metal cation, the resulting effect may differ depending on the synthesis or reaction conditions^[84]. With regard to dopant concentration, there is a consensus that at low amounts, the dopants act as trapping sites that can improve charge separation and introduce intermediate energy levels in the band gap that promote electron excitation at longer (visible light) wavelengths. At higher concentrations they can become recombination sites^[85]. Joshi et al.^[86] reported the adverse effect of doping TiO_2 with transition metal ions on photo-catalytic activity because of the formation of localized *d*-states in the band gap of TiO_2 . Localized *d*-states act as trapping sites that capture electrons from the conduction band or holes from the valence band. Hence, there often exists an optimum amount of dopant, which is typically in the order of 1 wt% or lower (TiO_2 basis). The influence of the structural environment of the dopant is illustrated by Sun et al., who did not observe visible light activity when the cations were present as surface complexes^[87]. The requirement for ion incorporation in the bulk lattice is also confirmed by Kang et al.^[88]. Metal ions that are not well incorporated in the lattice may block active sites at the surface and lead to lower activities.

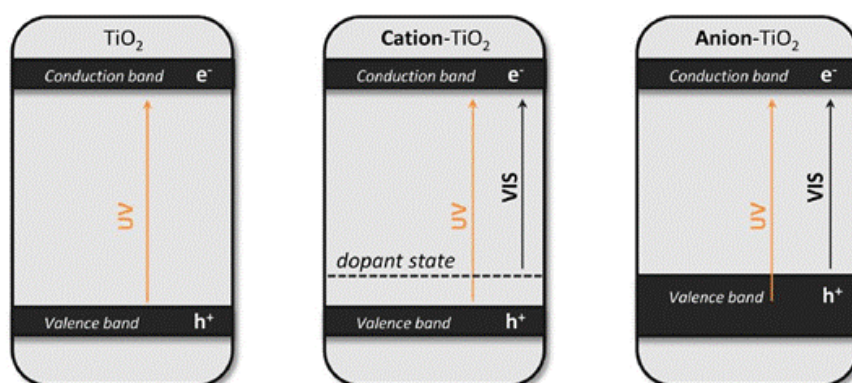


Figure 5. Schematic illustration of the effect of doping with cations (dopant energy level arbitrarily chosen) and anions on the band gap.

From a chemical point of view, TiO_2 doping is equivalent to the introduction of defect sites like Ti^{3+} into the semiconductor lattice, where the oxidation of Ti^{3+} species is kinetically fast compared with the oxidation of Ti^{4+} . The differences in photoactivity derive from the change in the diffusion length of the minority carriers^[89]. For optimal e^-/h^+ separation, the magnitude of the potential drop across the space-charge layer should not fall below 0.2 V^[90]. The dopant content directly influences the rate of e^-/h^+ recombination by the equation: $W = (2 \epsilon \epsilon_0 V_s / e N_d)$, where W is the thickness of the space-charge layer, ϵ is the static dielectric constant of the semiconductor, ϵ_0 is the static dielectric constant in a vacuum, V_s is the surface potential, N_d is the number of dopant donor atoms, and e is the electron charge^[91]. As the concentration of the dopant increases, the space-charge region becomes narrower and the electron hole pairs within the region are efficiently separated by the large electric field before recombination. However, when the concentration of doping is high, the space-charge region is very narrow so the penetration depth of light into TiO_2 greatly exceeds the width of the space-charge layer. Therefore, the rate of recombination of photo-generated electron-hole pairs in the semiconductor increases because there is no driving force to separate them. Consequently, there is an optimum concentration of dopant ions where the thickness of the space-charge layer is similar to the depth of light penetration.

One recent trend that emerged the last five to ten years is doping with metals from the lanthanide group of the periodic table. Especially doping with Ce is a promising approach. It has a high thermal stability, as well as adsorption selectivity that may improve adsorption of pollutants at the catalyst surface, as has been shown in the case of nitrite adsorption on 0.7 wt% Ce- TiO_2 ^[92]. Another special feature of Ce is that it acts as a good structural promoter. Ce doping leads to well-defined mesoporosity and an increased thermal stability of the anatase phase^[93], which is beneficial for gas phase applications that benefit strongly from increased surface area. Several researchers have observed a retardation in the crystal growth and a suppression of the thermal anatase to rutile recrystallization^[94]. This structural stabilizing effect is attributed to the formation of Ti-O-Ce species at the surface, as a consequence of the large atomic radius that prevents Ce from being incorporated in the TiO_2 lattice^[95]. A final

aspect of Ce doping is the increased visible light absorption. The $\text{Ce}^{3+}/\text{Ce}^{4+}$ redox potential (1.8 eV) lies within the TiO_2 band gap. Consequently, a d -shift is observed in the range of 400–500 nm after doping with Ce [96].

Transition metal doping: There are a number of issues associated with metal ion doping, related to the efficiency of subsequent photo-catalytic processes. Whereas the presence of metal dopants was found in some cases to enhance charge separation as well as interfacial charge transfer [97] in many other cases, the metal dopants actually resulted in rapid charge recombination through their switchable redox states, for example, $\text{Fe}^{3+} \leftrightarrow \text{Fe}^{2+}$ and thereby reducing the electron diffusion length and lifetime [98-100]. This is one of the reasons for the reduced quantum efficiency in many photo response-extended doped photocatalysts.

Grätzel et al. [101] studied the effect of doping TiO_2 with transition metals such as Fe, V, and Mo by electron paramagnetic resonance.

Choi et al. doped TiO_2 with 21 transition metal ions and investigated their photo-catalytic activities [102]. Visible-light photo-responses were observed for TiO_2 photocatalyst as a result of most of these metal ion doping. Extensive research on the enhancement of TiO_2 photo-catalytic activities has been performed through doping of transition and rare earth metal ions, especially for air and water sanitization applications [103,104]. Among the various metal ions studied by Choi et al., increased photo-catalytic activity was identified for Mo, V, Re, Ru, Fe, Rh, and Os ions doped TiO_2 [103]. Whereas Al and Co ions reduced the activity. Fe and Cu ions create additional energy levels near the valence band as well as conduction band of TiO_2 , which result in the trapping of both electrons and holes. Consequently, it is highly recommended to dope TiO_2 with either Fe or Cu ions to obtain superior photo-catalytic activity. Hashimoto et al. designed and fabricated Cu(II) and Fe(III) grafted TiO_2 photocatalysts for efficient visible-light induced decomposition of 2-propanol to CO_2 via acetone [104]. In this case, visible-light activation was caused by the interfacial charge transfer from the valence band holes to Cu(II) ions. Cu(I) ions formed by the reduction of Cu(II) also act as a multi-electron oxygen reduction catalyst. Fe(III)-grafted rutile TiO_2 displayed optical absorption in the visible region above 400 nm, which resulted from the interfacial charge transfer from the valence band of TiO_2 to the surface Fe(III) species.

Superior quantum efficiency of 22% was observed for Fe(III)/ TiO_2 in the visible-light region (400–530 nm), and photo-catalytic activity can be maintained up to 580 nm with a quantum efficiency of 10%. High performance of Fe(III)/ TiO_2 was attributed to the accumulation of photogenerated holes in the valence band of TiO_2 and the catalytic reduction of oxygen by photoreduced Fe(II) species on TiO_2 surface (**Figure 6**). Peng et al. investigated the photo-catalytic activity of Be doped TiO_2 [105]. They found that metal ion doping close to the surface improves charge carrier separation, whereas deep doping accelerates carrier recombination. These findings were in good agreement with the results of Choi et al. [103]. Wu et al. investigated the effects of transitional metal ions (Cr, Mn, Fe, Co, Ni and Cu) doping on the photo-catalytic activity of TiO_2 through the photo-catalytic oxidation of acetic acid [106]. Enhanced photo-catalytic activities were observed for Cu, Mn and Fe ions doped TiO_2 as they can trap electrons as well as holes, whereas Cr, Co and Ni ions doped samples were not much active as they can trap only one charge carrier. Dhanalakshmi et al. investigated the dye sensitized hydrogen production efficiency of Cu-modified TiO_2 and compared with that of Pt-doped compositions and the enhancing effect was found to be comparable [107].

A ten-fold enhancement in the hydrogen production efficiency was demonstrated at an optimum Cu-loading. Xu et al. [108] compared photo-catalytic activities of various (La, Ce, Er, Pr, Gd, Nd and Sm) rare earth metal ion doped TiO_2 . TiO_2 loaded with optimum dopant content demonstrated superior band-gap narrowing and visible-light photo-catalytic activities. As a result of its ability to transfer both electrons and holes to the surface Gd-ions doped TiO_2 was found to be the most photoactive.

Non-metal (anion) doping: Increasing visible light absorption by doping with anions has been considered since the end of the 1980s. Carbon, Fluorine, Sulfur, Boron, Phosphor and Halides are all known examples, but doping with nitrogen has attracted most attention since the first discovery of Sato et al. in 1986 [109]. It is easily incorporated in the TiO_2 lattice due to its low ionization potential and comparable atomic radius to oxygen [110]. There is a general hypothesis that incorporation of anions with lower electronegativity than oxygen in the TiO_2 lattice, results in an upward shift of the 2p-levels of the valence band and thus narrows the band gap, in contrast to cation doping that results in additional energy states within the band gap itself (**Figure 5**). At this point it is not 100% clear whether the N-related states are localized or intrinsically part of the band gap. Nitrogen can be easily introduced in the TiO_2 structure, due to its comparable atomic size with oxygen, small ionization energy and high stability. It was in 1986 when Sato discovered that addition of NH_4OH in a titania sol, followed by calcination of the precipitated powder, resulted in a material that exhibited a visible light response [111,112]. Later on, Asahi and co-workers [113] calculated the electronic band structures of TiO_2 containing different substitution dopants including C, N, F, P and S. Substitution doping with N narrowed the band gap most significantly because its p state mixed with the O 2p states. In addition, molecular dopants like NO and N_2 gave rise to bonding states below the O 2p valence band and anti-bonding states deep in the band gap (N_i and N_{its}) that were well screened and hardly interacted with the band states of TiO_2 . Model pollutants that have been reported to be effectively degraded by visible active titania photo-catalyst include phenols, methylene blue, methyl orange (although dyes have strong absorption in the visible range) and Rhodamine B, as well as several gaseous pollutants (e.g., volatile organic compounds, nitrogen oxides) [114].

For the efficient incorporation of nitrogen into TiO_2 either in the bulk or as a surface dopant, both dry and wet preparation methods have been adopted. However, the most versatile technique for the synthesis of N- TiO_2 nanoparticles is the sol-gel

method, which requires relatively simple equipment and permits fine control of the materials nanostructure, morphology and porosity. Simultaneous TiO₂ growth and N doping is achieved by hydrolysis of titanium alkoxide precursors in the presence of nitrogen sources. Typical titanium salts (titanium tetrachloride) and alkoxide precursors (including titanium tetra-isopropoxide, tetrabutyl orthotitanate) have been used. Nitrogen containing precursors used include aliphatic amines, nitrates, ammonium salts, ammonia and urea [115-117]. The synthesis route involves several steps; however, the main characteristic is that precursor hydrolysis is usually performed at room temperature. The precipitate is then dried to remove solvents, pulverized and calcined at temperatures from 200 to 600 °C.

N-doped TiO₂ was followed by other nonmetal doped titania photocatalysts such as carbon, sulfur, boron, phosphorus, fluorine and iodine. Sakthivel and Kisch [118] showed that C-doped TiO₂ was five times more active than N-doped TiO₂ toward the degradation of 4-chlorophenol by artificial light ($\lambda \geq 455$ nm). Periyat et al. successfully developed S-doped TiO₂ through modification of titanium isopropoxide with sulphuric acid. They found that formation of titanyl oxysulfate results in the retention of anatase at increased temperatures (≥ 800 °C) and that the presence of sulfur causes increased visible light photo-catalytic activity of the synthesized materials [119].

P-doped TiO₂ was prepared by a simple modified sol-gel method with hypophosphorous acid as a precursor, and it was found that P-TiO₂ significantly increased the surface area of the photocatalyst and consequently provided a higher content of surface hydroxyl groups, thus elevating photo-catalytic activity [120]. The phosphorus doping extended the spectral response's shift into the visible region, and represented more effective photo-catalytic degradation of the Methylene Blue (MB) and 4-chlorophenol (4CP) under visible light (>400 nm) irradiation.

Insertion of fluorine into the TiO₂ crystal lattice has also been reported to elevate the anatase to rutile phase transformation temperature. Padmanabhan et al. [121] successfully modified titanium isopropoxide with trifluoroacetic acid carrying out a sol-gel synthesis. The resulting material proved to be more photo-catalytically active than Evonik P25 while also retaining anatase at temperatures of up to 900 °C.

In general; the sol-gel process is one of the versatile methods to prepare nano-size materials. This technique does not require complicated instruments and provides simple and easy means for preparing nano-size particles. The incorporation of an active dopant in the sol during the gelation stage allows the doping elements to have a direct interaction with support, therefore, the material possesses catalytic or photo-catalytic properties. A typical preparation procedure by the sol-gel method of doped TiO₂ is shown in **Figure 6**. Titanium precursor such as Titanium Isopropoxide (TIP), Tetrabutyl Orthotitanate (TBOT), titanium tetra chloride, is mixed with dopant precursor dissolved in alcohol, followed by hydrolysis performed at the room or elevated temperature. The precipitate is dried usually at temperature range from 80 to 110 °C, pulverized to obtain xerogel and calcined in air at temperature from 200 to 600 °C (**Figure 7**).

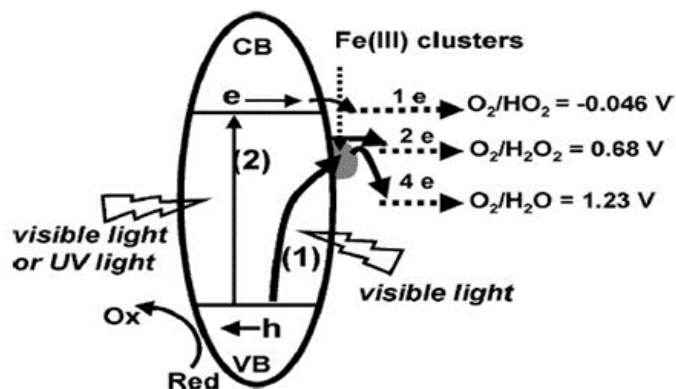


Figure 6. Schematic diagram illustrating the possible photo-catalytic mechanism of Fe(III)/TiO₂ involving interfacial electron transfer and multielectron oxygen reduction.

Heterojunction: Joining Different Semiconductors

Coupling of semiconductors having different band gap values is another method to efficiently utilize visible-light and enhancing the photo-catalytic activity. The necessary condition for coupling is that the conduction band level of at least one of the semiconductors must have a more negative value compared to the other. The electron injection mechanism in composite semiconductors can occur through the following mechanism (**Figure 8**). In the case of semiconductor hetero junctions, photogenerated electrons can be effectively transferred from the conduction band of one semiconductor to that of the other. The electron injection always occurs from the more negative conduction band to the less negative one.

There has been much interest in coupling different semiconductor particles with TiO₂, with coupled samples such as TiO₂-CdS, Bi₂S₃-TiO₂, TiO₂-WO₃, TiO₂-SnO₂, TiO₂-MoO₃, and TiO₂-Fe₂O₃ being reported [122-129].

Coupling of TiO₂ with CdS (band gap 2.4 eV) and SnO₂ (band gap 3.5 eV) for visible-light induced water splitting and purification were previously investigated [130,131]. In this case, the small band gap CdS (CB=-0.76 eV) cause visible-light sensitization, and inject

electrons to the conduction band of SnO_2 (CB=-0.34 eV), which results in an efficient electron-hole separation and an increase of photo-catalytic activity. Doong et al. reported very high photo-catalytic activity of CdS coupled TiO_2 towards the photo-catalytic decomposition of 2-chlorophenol [132]. The better photo-catalytic activity resulted from the electron injection from CdS to TiO_2 and hole injection from TiO_2 to CdS, which results in better charge separation. Kang et al. demonstrated the photodegradation of 4-chlorophenol using CdS- TiO_2 composite semiconductor [133]. The photo-catalytic activities of the composite were found to be very high in comparison to that of CdS and TiO_2 used separately.

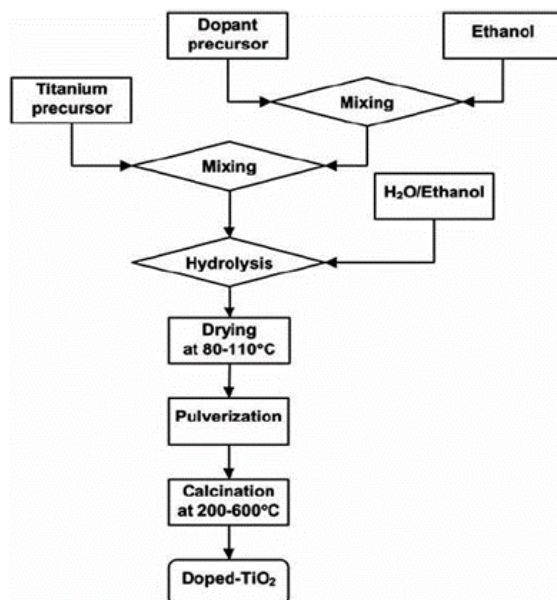


Figure 7. Typical procedure of doped- TiO_2 preparation by sol-gel method.

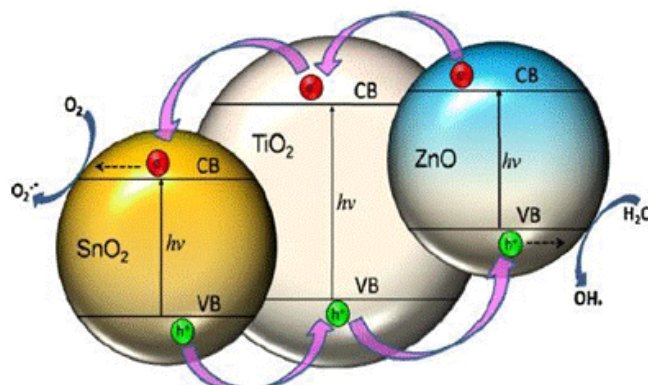


Figure 8. Electron transfer mechanism in composite semiconductor.

Uddin et al. [134] used an impregnation method to introduce a transition-metal oxide of ruthenium oxide (RuO_2) which possessed a high work function of about 6.1 eV on the sol-gel processed TiO_2 nanopowders. The resulting $\text{RuO}_2/\text{TiO}_2$ mesoporous heterojunction exhibited a significant enhancement in the photo-catalytic activity due to the improved separation of photogenerated electron-hole pairs resulting from the internal electric field. Several advantages can be achieved by adopting p-n junction: (1) more effective charge separation; (2) rapid charge transfer to the catalyst; (3) longer lifetime of the charge carriers; (4) separation of locally incompatible reduction and oxidation reactions in nanospace [135]. Furthermore, since the TiO_2 material is a well-known n-type material, Nickel Oxide (NiO) which shows a p-type semiconducting nature with a high band gap of about 3.86 eV [136], it is also expected to be a promising candidate on contact to TiO_2 since an additive pathway associated with the formation of an inner electrical field between the heterojunction which is favorable for the separation of the photo-generated electrons and holes to different semiconductors in the p-NiO/n- TiO_2 heterojunction structure, can be achieved. A few groups have had success in preparing a NiO/ TiO_2 heterojunction and the improvements in the resulting photo-catalytic activity as a mechanism of the p-n junction have been discussed briefly [137].

Bi_2S_3 nanoparticles with a direct band gap of 1.28 eV are a good material for the photosensitization of nanocrystalline TiO_2 . The conduction band of Bi_2S_3 nanoparticles is less anodic than the conduction band of TiO_2 and the valence band is more cathodic than the valence band of TiO_2 [138], enhancing electron injection from the excited state of Bi_2S_3 into TiO_2 . Bessekhoud et al. [125] studied a $\text{Bi}_2\text{S}_3/\text{TiO}_2$ junction prepared by precipitation of different concentrations of Bi_2S_3 onto TiO_2 . Bi_2S_3 absorbed a large portion of visible light and when the junction contained 10 wt% Bi_2S_3 , the absorbance started at 800 nm.

The coupled system WO_3/TiO_2 has been used as a photocatalyst for decades. Both the upper edge of the valence band and the lower edge of the conduction band of WO_3 are lower than those of TiO_2 , WO_3 can be excited by illumination with visible light

and the photogenerated holes can transfer from WO_3 to TiO_2 . Song et al. [126] observed that loading of WO_3 on the TiO_2 surface improved the decomposition of 1,4-dichlorobenzene in aqueous solution by up to 5.9 times compared with pure TiO_2 . Because the standard reduction potential between W(VI) and W(V) is only -0.03 V, it was deduced that electrons in the conduction band of TiO_2 could be easily accepted by WO_3 . The electrons in WO_3 would then be transferred to the oxygen molecules adsorbed on the surface of TiO_2 . Grandcolas et al. [127] reported porogen template assisted sol-gel synthesis of coupled rutile-anatase TiO_2 with a high surface area. It acted as a support for WO_3 , which extended the absorption to the visible region and improved the photo-catalytic performance.

Interestingly, this type of charge separation can also occur in polymorphic TiO_2 (i.e. co-presence of anatase and rutile). It has been suggested that the good photo-catalytic performance of commercial P25 (Evonik) is not only attributable to its nanocrystalline nature, but also to its polymorphic composition (roughly 80% anatase, 20% rutile). After the initial work of Bickley et al. [138] and several other researchers trying to unravel the synergy of anatase and rutile [139], Ohtani et al. concluded in 2010 that the different fractions of P25 behave independently, without any interaction [140]. However, one year later Su et al. [141] contradicted this finding in a convincing study that demonstrates the synergetic effect for anatase-rutile composites with an anatase content of at least 40% and rutile fraction of at least 20%. Their study was unique in that sense that different composite samples were prepared in which only the anatase/rutile ratio was altered. All other morphological parameters were kept constant. Since morphological parameters are ruled out of the equation, it can be expected that the synergy is an intrinsic catalytic property and thus applies to both liquid and gas phase reactions. A maximal synergetic effect was observed in their experiments for 60% anatase and 40% rutile, which was 50% higher compared to pure anatase [142].

Recently, Li et al. [130] synthesized a series of highly visible-light efficient semiconductors by combining N-doped ZnO with WO_3 , V_2O_5 and Fe_2O_3 . In these composite semiconductors, visible-light activation was achieved through nitrogen doping and the small band gap semiconductors such as WO_3 , V_2O_5 and Fe_2O_3 were responsible for effective electron-hole separation. Coupling of TiO_2 with WO_3 and V_2O_5 were found to be more effective compared to Fe_2O_3 due to carrier recombination on Fe_2O_3 . However, these composites were not suitable for hydrogen production due to the less negative position of WO_3 and V_2O_5 conduction bands.

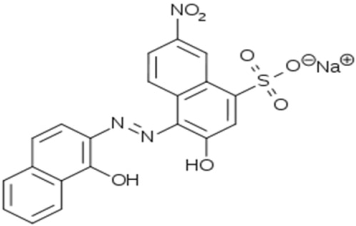
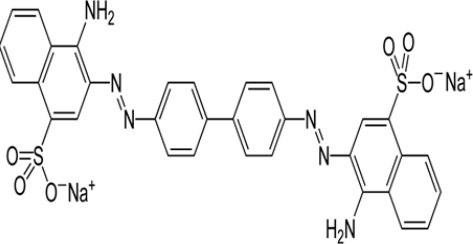
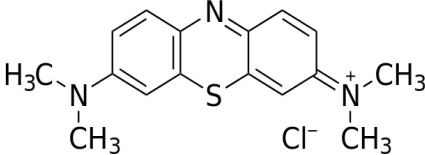
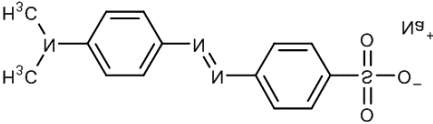
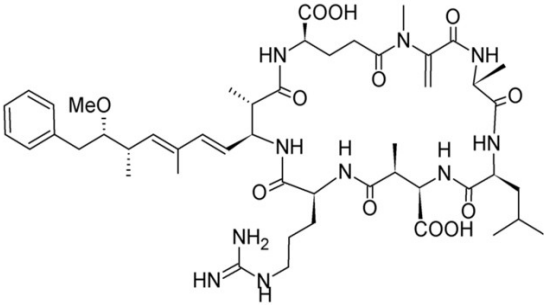
ENVIRONMENTAL APPLICATION OF PHOTO-CATALYSTS

Over the last two decades, photo-catalysis with TiO_2 nanoparticles has been shown useful for the degradation of wastewater pollutants. This process has several advantages including complete mineralization of organic pollutants like aliphatics, aromatics, polymers, dyes, surfactants, pesticides and herbicides to CO_2 , water and mineral acids, no waste solids to dispose of and mild temperature and pressure conditions. Photo-catalysis with TiO_2 nanoparticles uses two kinds of reaction systems, namely suspension and immobilized systems [143]. Because the reaction area was large, it allowed highly efficient decomposition of harmful organic substances, unpleasant odors and colored matters present in wastewater. Recently, increasing research activity has been dedicated to investigating photo-catalytic materials that differ from TiO_2 for detoxification of aqueous effluents, most aimed to achieve more efficient usage of solar light (**Figure 9**). A considerable variety of material alternatives to TiO_2 , most of them oxides but also some sulfides have been tested for aqueous pollutants degradation. Regarding pollutants, organic dyes are the most employed model compounds for photo-catalytic activity tests. The textile industry is a major consumer of water. It is estimated that it uses 378 billion liters per year in various processes such as mercerization, desizing, scouring, dyeing, and rinsing. With a total volume of wastewater of around 150 billion liters per year, the wastewater from textile production accounts for a large portion of the total industrial wastewater [144]. Colored industrial wastewaters may exhibit toxic, carcinogenic, and even mutagenic characteristics and as such present a serious hazard to aquatic organisms and humans. Among dyes, azo dyes are the largest group of synthetic dyes with estimated world annual production of around 500,000 tons [145] and are also the most abundant group that is discharged into the aquatic environment. However, it should be noted that, when using these kinds of molecules, dye sensitization of the semiconductor instead of direct excitation of the photocatalyst cannot be ruled out as a possible reaction mechanism (**Table 1**).



Figure 9. Industrial waste waters.

Table 1. Chemical structure, molecular formula and molecular weight of different dyes.

Dyes	MF	M.Wt (gm/mol)
 <p>Eriochrome Black T (EBT)</p>	C ₂₀ H ₁₂ N ₃ O ₇ Na	461.38
 <p>Congo Red (CR)</p>	C ₃₂ H ₂₂ N ₆ Na ₂ O ₆ S ₂	696.665
 <p>Methylene Blue (MB)</p>	C ₁₆ H ₁₈ ClN ₃ S	319.85
 <p>Methyl Orange (MO)</p>	C ₁₄ H ₁₄ N ₃ NaO ₃ S	327.33
 <p>Microcystin-LR (MC-LR)</p>	C ₄₉ H ₇₄ N ₁₀ O ₁₂	995.19

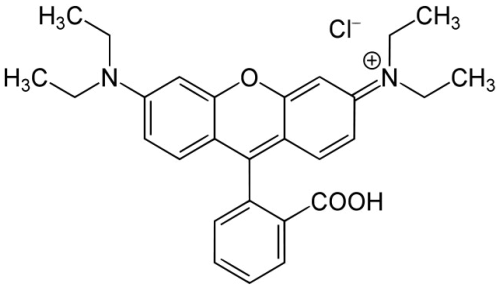
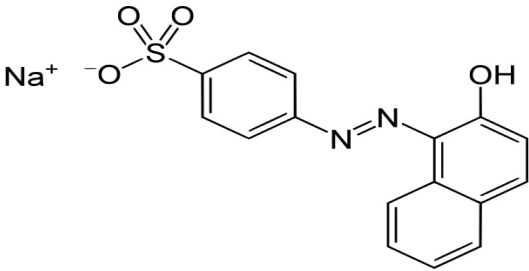
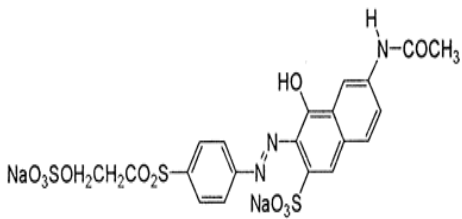
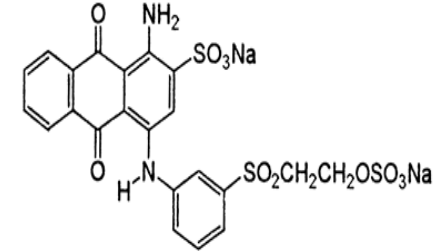
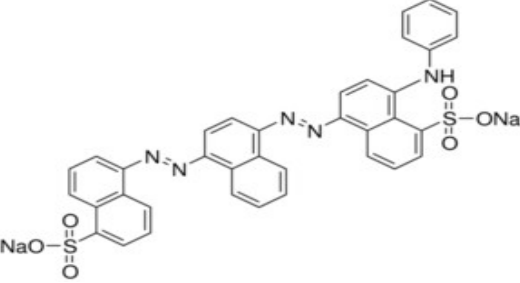
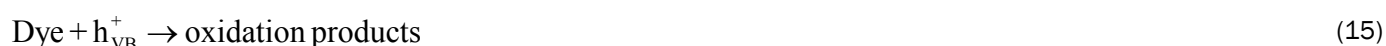
 <p>Rhodamine B (RhB)</p>	<p>C28H31ClN2O3</p>	<p>479.02</p>
 <p>Acid orange 7 (AO7)</p>	<p>C16H11N2NaO4S</p>	<p>350.32</p>
 <p>Reactive Orange (RO)</p>	<p>C20H17N3Na2O11S3</p>	<p>617.54</p>
 <p>Reactive blue 19 (RB)</p>	<p>C22H16N2Na2O11S3</p>	<p>626.55</p>
 <p>Acid black 24 (AB)</p>	<p>C36H23N5Na2O6S2</p>	<p>731.71</p>

Photo-Catalytic Degradation Mechanisms of Dye

Photo-catalytic oxidation: The mechanism of the process has been briefly summarized here. It is well established that conduction band electrons (e^-) and valence band holes (h^+) are generated when aqueous TiO_2 suspension is irradiated with light energy greater than its band gap energy (Eg, 3.2 eV). The photogenerated electrons could reduce the dye or react with electron acceptors such as O_2 adsorbed on the Ti(III)-surface or dissolved in water, reducing it to superoxide radical anion $O_2^{\cdot-}$. The photogenerated holes can oxidize the organic molecule to form R^+ , or react with OH^- or H_2O oxidizing them into OH^{\cdot} radicals.

Together with other highly oxidant species (peroxide radicals) they are reported to be responsible for the heterogeneous TiO_2 photodecomposition of organic substrates as dyes. According to this, the relevant reactions at the semiconductor surface causing the degradation of dyes can be expressed as follows:



The resulting $\cdot\text{OH}$ radical, being a very strong oxidizing agent (standard redox potential +2.8 V) can oxidize most of azo dyes to the mineral end-products. Substrates not reactive toward hydroxyl radicals are degraded employing TiO_2 photo-catalysis with rates of decay highly influenced by the semiconductor valence band edge position^[146]. The role of reductive pathways (Eq. (16)) in heterogeneous photo-catalysis has been envisaged also in the degradation of several dyes but in a minor extent than oxidation^[147].

Photosensitized oxidation: The mechanism of photosensitized oxidation (called also photo-assisted degradation) by visible radiation ($\lambda > 420$ nm) is different from the pathway implicated under UV light radiation. In the former case the mechanism suggests that excitation of the adsorbed dye takes place by visible light to appropriate singlet or triplet states, subsequently followed by electron injection from the excited dye molecule onto the conduction band of the TiO_2 particles, whereas the dye is converted to the cationic dye radicals ($\text{Dye}^{\cdot+}$) that undergoes degradation to yield products as follows^[148]:



The cationic dye radicals readily reacts with hydroxyl ions undergoing oxidation via reactions 13 and 14 or interacts effectively with O_2^- , HO_2^\cdot or HO^\cdot species to generate intermediates that ultimately lead to CO_2 (Eqs. (23–29)).



In experiments that are carried out using sunlight or simulated sunlight (laboratory experiments) it is suggested that both photooxidation and photosensitizing mechanism occurred during the irradiation and both TiO_2 and the light source are necessary for the reaction to occur. In the photo-catalytic oxidation, TiO_2 has to be irradiated and excited in near-UV energy to induce charge separation. On the other hand, dyes rather TiO_2 are excited by visible light followed by electron injection onto TiO_2 conduction band, which leads to photosensitized oxidation. It is difficult to conclude whether the photo-catalytic oxidation is superior to the photosensitizing oxidation mechanism, but the photosensitizing mechanism will help to improve the overall efficiency and make the photo bleaching of dyes using solar light more feasible^[149].

THE NEW PROMISING SEMICONDUCTORS IN PHOTO-DEGRADATION OF DYES

Methyl Orange (MO) dye in water is highly visible, even at very low concentrations, which hinders the penetration of light and therefore causes adverse effects on photosynthesis [150]. Congo Red (CR) was the first synthetic dye that could dye cotton directly. It is contained in wastewater effluents from the textile, printing and dyeing, paper, rubber and plastics industries [151]. CR is used in medicine as a biological stain and as an indicator since it turns from red-brown in a basic medium to blue in an acidic one [152]. It can also be used as a secondary gamma-ray dosimeter since its coloration decays with the intensity of radiation [153]. Therefore, the effective decolorization of dye-containing wastewater is an important and challenging task that must be approached. Three different commercially available TiO₂ nanoparticles were used: pure-phase anatase, pure-phase rutile, and mixed-phase preparation named Degussa P25 as semiconductor photocatalysts for the degradation of MO and CR dyes in an aqueous solution [154]. Since TiO₂ particles become photo-catalytically active by UV radiation, two sources of UV-A radiation were used-natural solar radiation which contains 3-5% UV-A and artificial, solar-like radiation, created by using a lamp. The optimal doses of TiO₂ of 500 mg/L for the CR and 1500 mg/L for the MO degradation were determined in experiments with the lamp and were also used in degradation experiments with natural solar light. The efficiency of each process was determined by measuring the absorbance at two visible wavelengths, 466 nm for MO and 498 nm for CR, and the Total Organic Carbon (TOC), i.e. decolorization and mineralization, respectively. In both cases, considerable potential for the degradation of CR and MO was observed total decolorization of the solution was achieved within 30-60 min, while the TOC removal was in the range 60-90%. CR and MO solutions irradiated without TiO₂ nanoparticles showed no observable changes in either decolorization or mineralization.

Zero valent silver nanoparticle deposited TiO₂ composite Ag/TiO₂ showed a good efficiency for the degradation of MB under the UV-C irradiation [155]. The photo-catalytic activity of Ag/TiO₂ essentially depends on the experimental conditions. The MB degradation rate increased with the increase in solution pH from 3 to 9. The decomposition of MB also increased with the increase in the mass of Ag/TiO₂ from 0.025 g to 0.1 g and on further increase in catalyst mass, negative results were obtained. An efficient sonophoto-catalytic degradation of reactive blue19 (RB 19) using sulfur-doped TiO₂ nanoparticles was reported recently [156]. In this method, coupling of ultrasound and photo-catalysis improved dye degradation through synergistic effect, which increased the amount of reactive radicals OH[•] and H₂O₂. It is also proposed that ultrasound increases the mass transport between the solution phase and catalyst surface, and de-agglomeration of particles increase the surface area of the catalyst. N-doped TiO₂ on glass spheres for Eriochrome Black-T decomposition [157], and CdO/TiO₂ coupled semiconductor for Reactive Orange degradation [158].

Recently, un-doped, Mo and V mono and co-doped nanocrystalline TiO₂ powders consisting of anatase with minor brookite and rutile phases were prepared by ultrasonic assisted sol-gel method [159]. The co-doped powder exhibited better visible light absorption behavior than the monodoped and un-doped TiO₂ powders (TMo_xV_y>TMo_x>TV_y>T>T⁺), because Mo⁶⁺ and V⁵⁺ dopant ions produce different energy levels within the band gap. In addition, as a result of charge compensation due to the substitution of dopants for Ti⁴⁺ in the TiO₂ crystal lattice can modify oxygen vacancies, they in combination with Ti³⁺ states contribute to the improvement of the photocatalyst responses toward visible light. UV and visible light photo-catalytic activity of the synthesized powders were tested for the decomposition of methylene blue and sulfamethoxazole under UV and visible light irradiation. It was observed that co-doped samples have enhanced activity than the rest of the prepared powders. This enhancement in activity was due to: (i) the composite nature of the sample which facilitated the interfacial charge transfer, (ii) the surface acidity and the high surface area via small crystallite size improving pollutant adsorption on the catalyst surface and providing abundant active reaction sites, (iii) the surface states and oxygen vacancies contributing to the increased absorption of light photons and (iv) the substituted dopant ions (Mo and V) acting as carrier trapping sites thus helping in reducing there combination of photogenerated charge carriers.

(Yb, N)-TiO₂ photocatalyst has been synthesized by sol-gel method combined with microwave chemical synthesis. Also, the efficiency of the (Yb, N)-TiO₂ as a photocatalyst for the degradation of Methylene Blue (MB) using visible light irradiation has been evaluated [160]. Compared with the P25, N-doped TiO₂ and Yb-doped TiO₂, the (Yb, N)-co-doped TiO₂ exhibits higher photoactivity under visible light. The significant enhancement in the photo-catalytic activity of the (Yb, N)-co-doped TiO₂ is attributed to the synergistic effect of Yb and N. The N dopant extended the absorption to the visible region and Yb dopant was beneficial for suppressing the recombination of photogenerated electrons and holes.

The preparation of xAl-3%In-TiO₂ photocatalyst by the sol-gel method was studied [161]. Aluminum and indium were simultaneously doped into anatase TiO₂ matrix by substituting Ti⁴⁺ ions. The BET specific surface area of the sample 0.5%Al-3%In-TiO₂ is higher than that of 3%In-TiO₂, due to restrained crystal growing and smaller pore size. Ti-O-Al and Ti-O-In structures are found in the TiO₂ lattice in the Al-In co-doped TiO₂. The co-doped xAl-3%In-TiO₂ materials have improved adsorption capacity and photo-catalytic activity. Total methyl orange de-coloration efficiency decreases from 100% to 85.9% on 0.5%Al-3%In-TiO₂ after 6 reaction cycles, as compared to de-coloration efficiency dropping from 66% to 45.2% on 3%In-TiO₂. Un-doped and several differently doped (with Fe³⁺, N, and g-Al₂O₃) TiO₂-nanoparticle based photocatalysts and those covered with ultra-small gold nanoparticles (AuNPs) were engineered [162]. Their photo-catalytic performance was studied by utilizing them for the liquid-phase decomposition of the model dye Methylene Blue (MB) under visible-light irradiation. Among various photocatalysts, Au/Al₂O₃-TiO₂ showed the best performance for the MB photodegradation. Deposited AuNPs on the surfaces of all photocatalysts existed as Au⁰, and their photo-catalytic enhancement arises from the synergetic co-operation of the electron trapping ability of the AuNPs and dopant-induced band gap narrowing of TiO₂. Among those, γ-Al₂O₃ doped TiO₂ nanoparticles covered with deposited AuNPs show the best photo-catalytic performance. Ni (1 wt%), Pt (1 wt%)- and [Ni (0.5 wt%)/Pt (0.5 wt%)]-doped TiO₂ nanoporous catalysts

have been successfully obtained through a facile two-step hydrothermal route [163]. TiO_2 crystallizes mostly in the anatase phase and acts as a mesoporous matrix. Meanwhile, Ni, Pt and Ni/Pt dopants form small nanoparticles (NPs) (3–95 nm in diameter) which are hosted by the TiO_2 framework. The resulting composites exhibit a rather large surface area, in the range of 186–200 m^2/g . The band gap energy reduces from 3.03 eV for the un-doped TiO_2 to 2.15 eV for the Pt-loaded TiO_2 . As a consequence, absorption expands toward the visible light range. The photodegradation of Rhodamine B dye in aqueous medium has been investigated under UV-vis light irradiation. Higher degradation rates are achieved (63% for Pt-, 57% for Ni and 54% for Ni/Pt-doped TiO_2 against 39% for un-doped TiO_2).

ZnO has been frequently considered as an alternative to TiO_2 for photo-catalytic applications, since it shows similar activity in certain conditions [164]. In general, higher photo-catalytic reaction rates were obtained with ZnO samples than with TiO_2 Degussa P25, in spite of the low surface area of the ZnO samples. The authors attributed this elevated efficiency to the structural characteristics of the ZnO photocatalysts, which preferentially expose the unstable (100) face. The coupling of ZnO with other semiconductor has been also attempted in order to improve its photo-catalytic properties. Thus, ZnO/ SnO_2 and ZnO/ ZnO_2 coupled oxides have been evaluated for photo-catalytic degradation of aqueous methyl orange (MO) solutions [165] which resulted in faster degradation kinetics with respect to ZnO itself. The deposition of Fe_2O_3 , WO_3 and CdS onto ZnO substrates also led to higher activities compared to bare ZnO [166]. The increase in activity in these coupled systems is ascribed to charge separation at the interface, as it has been described for other semiconductor couples [167]. Similar to TiO_2 , another limitation of ZnO is its wide band gap (3.2 eV), which restricts light absorption to the UV region [164]. A possible strategy to extend ZnO absorption to visible light may be the modification of its valence band position by anionic doping, as has been achieved for TiO_2 [168]. Nanodisks of ZnO and Co doped ZnO were synthesized by a facile wet chemical method and their structural, optical and photo-catalytic properties were studied [169]. The ZnO nanodisks and Co doped ZnO nanodisks exhibit very high photo-catalytic efficiency for sun light driven degradation of methyl orange dye.

The nanocrystalline Cu-doped TiO_2/ZnO composite powder with TiO_2/ZnO weight ratio of 7/3 and 3 wt% copper, calcined at 500 °C was synthesised via sol-gel process, characterized and evaluated [170]. This composite presented a red shift in the absorption wavelength, notably narrowing the band gap (about 2.2 eV) compared to the pure TiO_2 (around 3.32 eV) and ZnO (around 3.37 eV). The analysis revealed that this photocatalyst had favorable crystalline phase which affect photo-catalysis directly. The main aim was to analyse the sensitivity of photoactivity of Cu- TiO_2/ZnO toward degradation of two important dyes (methylene orange and methyl blue) under visible light irradiation. The maximum removal efficiency of: color: 83.35%, COD: 73.54% and TOC: 54.46% for MO degradation and color: 75.50%, COD: 68.00% and TOC: 46.41% for MB degradation.

CeO_2 has also received attention as a photocatalyst because of its interesting properties: stability under illumination and strong absorption of both UV and visible light. However, this material has been generally found to be less active than TiO_2 under UV irradiation [171]. However, in contrast with titania, this oxide can be activated by visible (violet) light. Ji et al. [172] prepared mesoporous CeO_2 photocatalyst using MCM-48 as a template in a replication process. The mesoporous materials showed a high surface area and a blue shift in their light absorption with respect to bulk CeO_2 , as observed in their UV-vis spectra. In the photo-catalytic degradation of Acid Orange 7 (AO7) under visible light, both bulk and mesoporous CeO_2 led to faster degradation of the dye than TiO_2 P25 from Degussa, but the mesoporous sample presented the best performance. No degradation of AO7 was observed in the absence of catalyst. More recently, the same group investigated the photo-catalytic degradation of AO7 under visible light ($\lambda > 420$ nm) over CeO_2 nanoparticles [173]. Higher activity is found in CeO_2 with respect to TiO_2 (P25), which is attributed to a higher adsorption capacity of the lanthanide oxide, with no comments on the influence of the different light absorption onset of both catalysts. The degradation of the dye Acidic Black over CeO_2 under solar irradiation has also been studied [174].

MoS_2 , as a two-dimensional structure, has a large specific surface area, strong absorption ability and the weak van der Waals gap, and shows many excellent properties such as intercalation, lubrication, anisotropy, chemical inertness, catalysis and so on [175]. As for its catalytic property, MoS_2 has been widely used to remove S and N from crude oil [176]. What's more, it has a potential application in photo-catalysis [177]. It is always used for combining with other semiconductors to form heterojunction structure with the purpose of improve the photo-catalytic activity of photocatalyst. TiO_2 - MoS_2 composites showed higher photo-catalytic efficiency for the photo-catalytic decolorization of Rhodamine B (RhB) aqueous solution under visible light irradiation [178].

There are several limitations to use nano- TiO_2 with high surface activity as photocatalyst in the photo-catalytic reactor. One is fast aggregation of TiO_2 in suspension leads to effective surface area decreased and furthers its catalytic efficiency reduction. Furthermore, a filtration step after photo-catalytic reaction is required because of TiO_2 suspension. Attempts have been made to immobilize TiO_2 on different supports like zeolites [179], clays [180], fiberglass [181], activated carbon [182], and carbon nanotube [183]. Incorporation of adsorbent into TiO_2 has been considered a practical way to enhance the activity. It not only collects pollutants from dilute solution or open air to the vicinity active site of TiO_2 , but also retains them to be degraded by additional illumination. Zeolites have high surface area and porous structure, which have been used as conventional adsorbents. The fine titanium oxide photocatalysts loaded on zeolite have opened possibilities for photo-catalytic degradation of various organic pollutants with low concentration [184].

A novel approach for the synthesis of $\text{TiO}_2/\text{MoS}_2$ @zeolite photocatalyst was developed by ultrasonic assisted hydrothermal method using micro- MoS_2 as the photosensitizer [185]. The as prepared $\text{TiO}_2/\text{MoS}_2$ @zeolite photocatalysts show highly enhanced

photo-catalytic activity for degradation of MO under simulated solar light irradiation compared to that of Degussa P25 photocatalyst. MoS₂ in the composites acted as an electron donor for the interfacial electron transfer, and thus enhanced the separation of the photo-generated electron/hole pairs. The micro-/nano-MoS₂ formed in the hydrothermal process can promote the formation of superoxide radical anions (O₂^{•-}) in photo-catalytic reaction and the superoxide radical anions is the mainly oxidation species in the photo-catalytic reaction. Jiang et al. recently reported a novel ternary photocatalyst composed of TiO₂-In₂O₃ nanocrystals decorated with graphitic carbon nitride g-C₃N₄ for dye degradation and H₂ evolution^[186]. These ternary composites exhibited the highest RhB degradation rate, which is 6.6 times higher than that of g-C₃N₄. H₂-generation rate was 48 times of the pure g-C₃N₄. They attributed the enhanced photo-catalytic activity to efficient interfacial transfer of photogenerated electrons and holes among TiO₂, In₂O₃ and g-C₃N₄. Other recent developments in the area of visible-light induced environmental cleaning involve the use of graphene oxide titania GO-TiO₂ composites for Microcystin-LA removal^[187]. An α-Fe₂O₃-TiO₂/fly ash cenospheres (FAC) composite photocatalyst was prepared by depositing α-Fe₂O₃ onto floating TiO₂/FAC, which was synthesized via a simple sol-gel method^[188]. Rhodamine B was selected as the model substance for photo-catalytic reactions to evaluate catalytic ability. Results showed that the degradation efficiency was close to 100% within 1 h. Active species measurements indicated that •OH served as the dominating active species that played a key function in the reaction. A possible photo-catalytic degradation mechanism of α-Fe₂O₃-TiO₂/FAC was also discussed based on experimental results.

Bismuth tungstate (Bi₂WO₆), with suitable band gap and intrinsic structure, has captured considerable attention for its photo-catalytic effect on pollutant decomposition under visible light irradiation^[189]. However, the practical application of Bi₂WO₆ is limited by its low photocarriers separation efficiency. Remarkable improvement of photo-catalysis under simulated sunlight irradiation was achieved by employing Bi₂WO₆/TiO₂/Pt composite photocatalyst^[190]. The high photo-catalytic performance benefited from the increased light harvesting efficiency owing to the excitation of both TiO₂ and Bi₂WO₆ and the enhanced quantum yield due to the heterojunction between Bi₂WO₆ and TiO₂ as well as the Schottky barrier between TiO₂ and Pt. The superoxide radical originated from the electro-reduction of dissolved oxygen with photogenerated electrons was the main reactive oxygen species in Bi₂WO₆/TiO₂/Pt photo-catalytic process, and the hydroxyl radical derived from the reaction of holes and H₂O was also responsible for pollutant degradation.

CuCrO₂/TiO₂ composite was prepared using hydrothermal synthesis and spin-coating method^[191]. The photo-catalytic performance of CuCrO₂/TiO₂ was evaluated by degrading MB under UV irradiation. Both the degradation efficiency and apparent first-order rate constant of CuCrO₂/TiO₂ were enhanced in comparison to pure TiO₂. The enhanced photo-catalytic activity could be attributed to a better separation efficiency of photogenerated electron-hole pairs, which caused by the formation of p-n heterojunctions in CuCrO₂/TiO₂. The proposed photo-catalytic mechanism of CuCrO₂/TiO₂ was discussed for the first time.

Recently, magnetic composite particles that contain TiO₂ were developed as heterogeneous photocatalysts^[192]. These magnetic photocatalysts can be recovered by applying an external magnetic field and reused^[193]. Spinel ferrite is a good candidate material for use in supports for the photo-catalytic degradation of dyes or organic compounds^[194]. Effects of ferrite materials as supports (CoFe₂O₄, NiFe₂O₄, and Fe₃O₄) on nano-TiO₂ were synthesized by co-precipitation and elucidated by their use in the oxidation of methylene blue^[195,196].

The crystalline phase of TiO₂ onto magnetic MFe₂O₄ was formed by anatase and rutile. TiO₂/CoFe₂O₄ exhibited the strongest magnetic property of the prepared catalysts, and the photo-catalytic efficiencies followed the order TiO₂/CoFe₂O₄>TiO₂/NiFe₂O₄>TiO₂/Fe₃O₄. MB de-colorization was enhanced with the amount of TiO₂ on the photocatalyst, and was moderately affected by the extent of structural distortion of ferrite supports.

CONCLUSION

Semiconductor photo-catalysis involves the formation of electron-hole pairs, which is initiated by band gap excitation of the semiconductor particle. Photo-catalysis appears to be promising as a route for selective synthetic transformations or as an advanced oxidation process for environmental cleanup. Over the past few decades, continuous breakthroughs in the synthesis and modification of TiO₂ have realized new properties and applications with improved performance. In this paper, an overview of the properties, modification and selected applications of TiO₂ as well as its novel prospects is presented. Some of the major problems associated with photo-catalysis are rapid charge recombination and back reaction and an inability to use visible light efficiently. Addition of electron donors can enhance photo-catalytic activity by irreversibly reacting with valence band holes to prevent charge recombination. Doping of TiO₂ can inhibit charge recombination and expand its photo-response to the visible region through the formation of impurity energy levels. Coupling of semiconductors can also expand the light response of TiO₂ to the visible region. Novel modifications of TiO₂ and photodegradation mechanism of dye have been reviewed.

REFERENCES

1. William G, et al. The Chemistry of Water Treatment Processes Involving Ozone, Hydrogen Peroxide and Ultraviolet Radiation. Ozone: Science & Engineering. J Int Ozone Associat 1987; 9: 335-352.
2. National Water Research Institute. Treatment Technologies for Removal of Methyl Tertiary Butyl Ether (MTBE) from Drinking Water: Chapter III Advanced Oxidation Processes 2000.

3. Munter, et al. Advanced Oxidation Processes-Current Status and Prospects. *Proc Estonian Acad Sci Chem* 2001; 50: 59-80.
4. Brillasa E, et al. Aniline mineralization by AOP's: anodic oxidation, photocatalysis, electro-Fenton and photoelectro-Fenton processes. *Appl Catal B: Environ* 1998; 16: 31-42.
5. Audenaert WTM, et al. Application of a mechanistic UV/hydrogen peroxide model at full-scale: Sensitivity analysis, calibration and performance evaluation. *Chem Eng J* 2011; 171: 113-126.
6. Matthews RW. *Photochemical Conversion and Storage of Solar Energy*, Pelizzetti E, Schiavello M, Eds., Kluwer: Dordrech, 1991.
7. Pichat P, et al. Purification/deodorization of indoor air and gaseous effluents by TiO₂ photocatalysis. *Catal Today* 2000; 63: 363-369.
8. Robert D, et al. Heterogeneous photocatalytic degradation of 3-nitroacetophenone in TiO₂ aqueous suspension. *Photochem Photobiol: Chem* 2003; 156: 195-200.
9. Kamat P. TiO₂ Nanostructures: Recent Physical Chemistry Advances. *J Phys Chem Lett* 2012; 116: 11849-11851.
10. Kim TK, et al. Development of surface coating technology of TiO₂ powder and improvement of photocatalytic activity by surface modification. *Thin Solid Films* 2005; 475: 171-177.
11. Aboul-Gheit AK, et al. Different outlet for preparing nano-TiO₂ catalysts for the photodegradation of Black B dye in water. *Egypt J Petrol* 2014; 23: 339-348.
12. Bhatkhande DS, et al. Photocatalytic degradation for environmental applications - a review. *J Chem Technol Biotechnol* 2001; 77: 102-116.
13. Pirkanniemi K and Sillanpa M. Heterogeneous water phase catalysis as an environmental application: a review. *Chemosphere* 2002; 48: 1047-1060.
14. Huang A, et al. Photocatalytic Degradation of Triethylamine on Titanium Oxide Thin Films. *J Catal* 1999; 188: 40-47.
15. Arabatzis IM, et al. Preparation, characterization and photocatalytic activity of nanocrystalline thin film TiO₂ catalysts towards 3,5-dichlorophenol degradation. *J Photochem Photobiol A* 2002; 149: 237-245.
16. Varghese OK, et al. Extreme Changes in the Electrical Resistance of Titania Nanotubes with Hydrogen Exposure. *Adv Mater* 2003; 15: 624-627.
17. Wen BM, et al. Depositional Characteristics of Metal Coating on Single-Crystal TiO₂ Nanowires. *J Phys Chem B* 2005; 109: 12372-12375.
18. Wu JM and Qi B. Low-Temperature Growth of a Nitrogen-Doped Titania Nanoflower Film and Its Ability to Assist Photodegradation of Rhodamine B in Water. *J Phys Chem C* 2007; 111: 666-673.
19. Yi GR, et al. Ordered Macroporous Particles by Colloidal Templating. *Chem Mater* 2001; 13: 2613-2618.
20. Carp O, et al. Photoinduced reactivity of titanium dioxide. *Prog Solid State Chem* 2004; 32:33-177.
21. Chen X and Mao SS. *Titanium Dioxide Nanomaterials: Synthesis, Properties, Modifications, and Applications*. *Chem Rev* 2007; 107:2891-2959.
22. Mashid S, et al. Synthesis of TiO₂ nanoparticles by hydrolysis and peptization of titaniumisopropoxide solution, Semiconductor physics. *Quant Electron Optoelectron* 2006; 9: 65-68.
23. Jian S and Xudong W. Growth of rutile titanium dioxide nanowires by pulsed chemical vapour deposition. *Cryst Growth Des* 2011; 11: 949-954.
24. Bahadur N, et al. Selective gas sensing response from different loading of Ag in sol-gel mesoporous tittania powders. *Sensors Actuators B*. 2011; 159: 112-120.
25. Song S, et al. Structural, Electrical and optical properties of ITO films with a thin TiO₂ seed layer prepared by RF magnetron sputtering. *Vacuum* 2009; 8: 1091-1094.
26. Shen X, et al. Microemulsion-mediated solvothermal synthesis and photocatalytic properties of crystalline titania with controllable phases of anatase and rutile. *J Hazard Mater* 2011; 192: 651-657.
27. Uzunova-Bujnova M, et al. Crystal structure morphology and pphotocatalytic activity of modified TiO₂ films. *Catal Today* 2010; 151:14-20.
28. Asif Ali Tahir TA, et al. Enhancement of photoelectrochemical performance of AACVD-produced TiO₂ electrodes by microwave irradiation while preserving the nanostructure. *Chem Vap Dep* 2012; 18: 107-111.
29. Tanaka Y, et al. Influence of coil current modulation on TiO₂ nanoparticle synthesis using pulse-modulated induction thermal plasmas. *Thin Solid Films* 2011; 519: 7100- 7105.
30. Oh JK, et al. Synthesis of phase-and shape controlled TiO₂ nanoparticles via hydrothermal process. *J Indust Engg Chem* 2009;

15: 270 - 274.

31. Melis A, et al. Deposition of photocatalytically active TiO₂ films assisted hydrothermal synthesis. *Nanotechnology*. 2012; 23: 165603.
32. Zhang Y, et al. Synthesis and electro chemical studies of a layered spherical TiO₂ through low temperature solvothermal method. *Electro Acta* 2009; 54: 4079 - 4083.
33. Zhao Y, et al. Synthesis and optical properties of TiO₂ nanoparticles. *Mater Letter* 2007; 61: 79-83.
34. Tan W, et al. Preparation of nanocrystalline TiO₂ thin film at low temperature and its application in dye-sensitized solar cell. *Solid State Electrochem* 2009; 13: 651-656.
35. Arami A, et al. Sonochemical preparation of TiO₂ nanoparticles. *Mat Let* 2007; 61: 4559-4561.
36. Corradi AB, et al. Conventional and Microwave-hydrothermal Synthesis of TiO₂ Nanopowders. *J Am Ceram Soc* 2005; 88: 2639-2641.
37. Gomez R, et al. Pt-Sn/Al₂O₃ sol-gel catalysts: Catalytic properties. *J Mol Catal A* 1996; 109: 55-66.
38. Sonawane RS and Dongare MK. Sol-gel synthesis of Au/TiO₂ thin films for photocatalytic degradation of phenol in sunlight. *J Mol Catal A* 2006; 243: 68-76.
39. MacKenzie JD. Sol-Gel Research—Achievements Since 1981 and Prospects for the Future. *J Sol-Gel Sci Techn* 2003; 26: 23-27.
40. Klein LC. Sol-gel optical-materials. *Annu. A Review of Photocatalysts Prepared by Sol-Gel Method for VOCs Removal. Rev Mater Sci* 1993; 23: 437-452.
41. Klein LC and Woodman RH. Porous Ceramic Mater. 1996; 115: 109-124.
42. Chen X and Mao SS. Titanium dioxide nanomaterials: synthesis, properties, modifications, and applications. *Chem Rev* 2007; 107: 2891-2906.
43. Fujishima A and Honda K. Electrochemical photolysis of water at a semiconductor electrode. *Nature*. 1972; 238: 37-38.
44. Diebold U. The surface science of titanium dioxide. *Surf Sci Rep* 2003; 28: 53-229.
45. Carp O, et al. Photoinduced reactivity of titanium dioxide. *Progg. Solid state chem* 2004; 32: 33-177.
46. Jho AK and Prasad K. Possible protection of silver nanoparticles against salt by using rhamnolipid. *Colloids surf B* 2010; 5: 330-334.
47. Burns A, et al. Sol-Gel Synthesis and Characterization of Neodymium-Ion Doped Nanostructured Titania Thin Films. *Mater Res Soc Symp* 2002; 703: 193-197.
48. Zhu Y, et al. The synthesis of nanosized TiO₂ powder using a sol-gel method with TiCl₄ as a precursor. *Mater Sci* 2000; 16: 4049-4054.
49. Di Paola A, et al. Photocatalytic activity of nanocrystalline TiO₂ (brookite, rutile and brookite-based) powders prepared by thermohydrolysis of TiCl₄ in aqueous chloride solutions. *Colloids Surf A* 2008; 7: 366-376.
50. Ghows N and Enterzari MH. Ultrasound with low intensity assisted the synthesis of nanocrystalline TiO₂ without calcinations. *Ultrason Sonochem* 2010; 17: 878-883.
51. Diebold U. The surface science of titanium dioxide. *Surf Sci Rep* 2003; 28: 53-229.
52. Carp O, et al. Microvolume TOC Analysis as Useful Tool in the Evaluation of Lab Scale Photocatalytic Processes. *Prog Solid State Chem* 2004; 32: 33-177.
53. Hosseinnia A, et al. Photo-catalytic Degradation of Organic Dyes with Different Chromophores by Synthesized Nanosize TiO₂ Particles. *World Appl Sci J* 2010; 8: 1327-1332.
54. Slamet H, et al. Effect of copper speceios in a photocatalytic synthesis of ethanol from carbon dioxide over copper doped titania. *World Appl Sci J* 2009; 6: 112-122.
55. Shahruz N and Hossain MM. Synthesis and size-control of TiO₂ photocatalyst nanoparticles preparation using sol-gel method. *World appl sci j* 2011; 12: 1981-1986.
56. Shaheed MA and Hussein FH. Synthesis and photocatalytic activity of TiO₂ Nanoparticles. *J Babylon Univ/Pure and Appl Sci* 2012; 1.
57. Venkatachalam N, et al. Sol-gel preparation and characterization of nanosize TiO₂; Its photocatalytic performance. *Mater Chem Phys* 2007; 104: 454-459.
58. Del Ángel-Sanchez K, et al. Photocatalytic degradation of 2,4-dichlorophenoxyacetic acid under visible light: Effect of synthesis route. *Mater Chem Phys* 2013; 13: 423-430.

59. Albano C, et al. Synthesis and characterization of nanostructures: MWCNTf/TiO₂ and MWCNTf/TiO₂/Hap. *Macromolecular Symposia* 2012; 321-322: 76-79.
60. Liu Y J, et al. Comparative examination of titania nanocrystals synthesized by peroxy titanate approach from different precursors. *J Colloid Interface Sci* 2008; 322: 497-504.
61. Sasirekha N, et al. Synthesis of TiO₂ sol in a neutral solution using TiCl₄ as a precursor and H₂O₂ as an oxidizing agent. *Thin Solid Films* 2009; 518: 43-48.
62. Liu T X, et al. TiO₂ hydrosols with high activity for photocatalytic degradation of formaldehyde in a gaseous phase. *J Hazard Mater* 2008; 152: 347-355.
63. Seok SI, et al. Colloidal TiO₂ nanocrystals prepared from peroxotitanium complex solutions: Phase evolution from different precursors. *J Colloid Interface Sci* 2010; 346: 66-71.
64. Lu J, et al. Synthesis and characterization of TiO₂ nanopowders from peroxotitanium solutions. *Mater Chem Phys* 2009; 115: 142-146.
65. Niederberger M and Garnweitner G. Organic Reaction Pathways in the Nonaqueous Synthesis of Metal Oxide Nanoparticles. *Chem Eur J* 2006; 12: 7282-7302.
66. Hay JN and Raval HM. Synthesis of Organic-Inorganic Hybrids via the Non-hydrolytic Sol-Gel Process. *Chem Mater* 2001; 13: 3396-3403.
67. Mutin PH and Vioux A. Nonhydrolytic Processing of Oxide-Based Materials: Simple Routes to Control Homogeneity, Morphology, and Nanostructure. *Chem Mater* 2009; 21: 582-596.
68. Vioux A. Nonhydrolytic Sol-Gel Routes to Oxides. *Chem Mater* 1997; 9: 2292-2299.
69. Arnal P, et al. A Solution Chemistry Study of Nonhydrolytic Sol-Gel Routes to Titania. *Chem Mater* 1997; 9: 694-698.
70. Aboulaich A, et al. Reactive and Organosoluble Anatase Nanoparticles by a Surfactant-Free Nonhydrolytic Synthesis. *Chem Mater* 2010; 22: 4519-4521.
71. Watanabe N, et al. Preparation of water-dispersible TiO₂ nanoparticles from titanium tetrachloride using urea hydrogen peroxide as an oxygen donor. *Cryst Eng Comm* 2013; 15: 10533-10540.
72. Sugimoto T. Formation of Monodispersed Nano- and Micro-Particles Controlled in Size, Shape, and Internal Structure. *Chem Eng Technol* 2003; 26: 313-321.
73. Eiden-Assmann S, et al. Synthesis and Characterization of Porous and Nonporous Monodisperse Colloidal TiO₂ Particles. *Chem Mater* 2004; 16: 6-11.
74. Han C, et al. Facile preparation of controllable size monodisperse anatase titania nanoparticles. *Chem Commun* 2012; 48: 1860-1862.
75. Kolasinski KW. *Surface Science - Foundations of Catalysis and Nanoscience*, 2nd ed., John Wiley & Sons Ltd, West Sussex, England 2009.
76. Van Gerven T, et al. A review of intensification of photo-catalytic processes. *Chem Eng Process* 2007; 46: 781-789.
77. Pelaez M, et al. A review on the visible light active titanium dioxide photocatalysts for environmental applications, *Appl Catal B* 2012; 125: 331-349.
78. Cho E, et al. First-principles study of point defects in rutile TiO_{2-x}. *Phys Rev B* 2006; 73: 193-202.
79. Justicia I, et al. Self-doped titanium oxide thin films for efficient visible light photocatalysis: An example: Nonylphenol photodegradation. *Sens. Actuators B: Chem* 2005; 109: 52-56.
80. Nakamura I, et al. Role of oxygen vacancy in the plasma-treated TiO₂ photocatalyst with visible light activity for NO removal. *J Mol Catal A* 2000; 161: 205-212.
81. Hamdy MS, et al. Surface Ti³⁺-Containing (blue) Titania: A Unique Photocatalyst with High Activity and Selectivity in Visible Light-Stimulated Selective Oxidation. *ACS Catal* 2012; 2: 2641-2647.
82. Etacheri V, et al. Oxygen Rich Titania: A Dopant Free, High Temperature Stable, and Visible-Light Active Anatase Photocatalyst. *Adv Funct Mater* 2011; 21: 3744-3752.
83. Mor GK, et al. A review on highly ordered, vertically oriented TiO₂ nanotube arrays: Fabrication, material properties, and solar energy applications. *Solar Energy Mater Solar Cell* 2006; 90: 2011-2075
84. Burda C, et al. Enhanced Nitrogen Doping in TiO₂ Nanoparticles. *Nano Lett* 2003; 3: 1049-1051.
85. Choi J, et al. Effects of Single Metal-Ion Doping on the Visible-Light Photoreactivity of TiO₂. *J Phys Chem C* 2010; 114: 783-792.
86. Choi WY, et al. The Role of Metal Ion Dopants in Quantum-Sized TiO₂: Correlation between Photoreactivity and Charge

- Carrier Recombination Dynamics. *J Phys Chem* 1994; 98: 13669-13679.
87. Joshi MM, et al. Visible light induced photoreduction of methyl orange by N-doped mesoporous titania. *Appl Catal A General* 2009; 357: 26-33.
 88. Sun B, et al. Visible Light Cr (VI) Reduction and Organic Chemical Oxidation by TiO₂ Photocatalysis. *Environ Sci Technol* 2005; 39: 6251-6259.
 89. Kang MS. The superhydrophilicity of Al-TiO₂ nanometer sized material synthesized using a solvothermal method. *Mater Lett* 2005; 59: 3122-3127.
 90. Maruska HP and Ghosh AK. Transition-metal dopants for extending the response of titanate photoelectrolysis anodes. *Sol Energy Mater* 1979; 1: 237-247.
 91. Gautron J, et al. Correlation between the non-stoichiometry of titanium dioxide and its photoelectrochemical behavior. *Faraday Discuss Chem Soc* 1981; 70: 81-91.
 92. Fox MA and Dulay MT. Heterogeneous Photocatalysis. *Chem Rev* 1993; 93: 341-357.
 93. Xu AW, et al. The Preparation, Characterization, and their Photocatalytic Activities of Rare-Earth-Doped TiO₂ Nanoparticles. *J Catal* 2002; 207: 151-157.
 94. Xiao J, et al. Preparation, phase transformation and photocatalytic activities of cerium-doped mesoporous titania nanoparticles. *J Solid State Chem* 2006; 179: 1161-1170.
 95. Silva AMT, et al. Ce-doped TiO₂ for photocatalytic degradation of chlorophenol. *Catal Today* 2009; 144: 13-18.
 96. Liu Z, et al. Preparation and characterization of cerium oxide doped TiO₂ nanoparticles. *J Phys Chem Solids* 2005; 66: 161-167.
 97. Sato S, Nakamura R, and Abe S. Visible-light sensitisation of TiO₂ photocatalysts by wet-method N doping. *Appl Catal A* 2005; 284: 131-137.
 98. Nah YC, et al. Nitrogen doping of nanoporous WO₃ layers by NH₃ treatment for increased visible light photoresponse. *Nanotechnol* 2010; 21: 105704.
 99. Teoh WY, et al. Progress in Heterogeneous Photocatalysis: From Classical Radical Chemistry to Engineering Nanomaterials and Solar Reactors. *J Phys Chem Lett* 2012; 3: 629-639.
 100. Kamat PV. Manipulation of Charge Transfer Across Semiconductor Interface. A Criterion That Cannot Be Ignored in Photocatalyst Design. *J Phys Chem Lett* 2012; 3: 663-672.
 101. Kamat PV. Graphene-Based Nanoarchitectures. Anchoring Semiconductor and Metal Nanoparticles on a Two-Dimensional Carbon Support. *J Phys Chem Lett* 2010; 1: 520-527.
 102. Grätzel M and Howe RF. Electron paramagnetic resonance studies of doped titanium dioxide colloids. *J Phys Chem* 1990; 94: 2566-2572.
 103. Choi W, et al. The role of metal ion dopants in quantum-sized TiO₂: correlation between photoreactivity and charge carrier recombination dynamics. *J Phys Chem* 1994; 84: 13669.
 104. Litter M. Heterogeneous photocatalysis: Transition metal ions in photocatalytic systems. *Appl Catal B* 1999; 23: 89-114.
 105. Dvoranova D, et al. Investigation of metal doped- titanium dioxide photocatalysts. *Appl Catal B* 2002; 37: 91.
 106. Yu H, et al. An Efficient Visible-Light-Sensitive Fe(III)-Grafted TiO₂ Photocatalyst. *J Phys Chem C* 2010; 114: 16481.
 107. Peng S, et al. Effect of Be²⁺ doping TiO₂ on its photocatalytic activity. *Chem Phys Lett* 2004; 398: 235.
 108. Wu X, et al. A combined DFT and restricted open-shell configuration interaction method including spin-orbit coupling: Application to transition metal L-edge X-ray absorption spectroscopy. *J Chem Phys* 2004; 20: 138.
 109. Dhanalakshmi K, et al. Dye sensitized hydrogen evolution from water. *Int J Hydrogen Energy* 2001; 26: 669-674.
 110. Sato S. Photocatalytic activity of NO_x-doped TiO₂ in the visible light. *Chem Phys Lett* 1986; 123: 126-128.
 111. Serpone N. Relative photonic efficiencies and quantum yields in heterogeneous photocatalysis. *J Photochem Photobiol A* 1997; 104: 1-12.
 112. Asahi R, et al. Visible-light photocatalysis in nitrogen-doped titanium oxides. *Sci* 2001; 293: 269-271.
 113. Zhang J, et al. Development of modified N doped TiO₂ photocatalyst with metals, nonmetals and metal oxides. *Energy Environ Sci* 2010; 3: 715-726.
 114. Mitoraj D and Kisch K. On the Mechanism of Urea-Induced Titania Modification. *Chem- A Eur J* 2010; 16: 261-269.
 115. Jagadale TC, et al. N-Doped TiO₂ Nanoparticle Based Visible Light Photocatalyst by Modified Peroxide Sol-Gel Method. *J Phys Chem C* 2008; 112: 14595-14602.

116. Qiu X, et al. Synthesis and Characterization of Nitrogen-Doped Group IVB Visible-Light-Photoactive Metal Oxide Nanoparticles. *Adv Mater* 2007; 19: 3995-3999.
117. Sakthivel S and Kisch H. Daylight photocatalysis by carbon-modified titanium dioxide. *Angew Chem Int Ed*, 2003; 42: 4908-4911.
118. Periyat P, et al. Improved High-Temperature Stability and Sun-Light-Driven Photocatalytic Activity of Sulfur-Doped Anatase TiO₂. *J Phy Chem C* 2008; 112: 7644-7652.
119. Lin L, et al. Photocatalytic properties of phosphor-doped titania nanoparticles. *Appl Catal B* 2007; 75: 52-58.
120. Padmanabhan SC, et al. A Simple Sol-Gel Processing for the Development of High-Temperature Stable Photoactive Anatase Titania. *Chem Mater* 2007; 19: 4474-4481.
121. Vogel R, et al. Quantum-Sized PbS, CdS, Ag₂S, Sb₂S₃, and Bi₂S₃ Particles as Sensitizers for Various Nanoporous Wide-Bandgap Semiconductors. *J Phys Chem* 1994; 98: 3183-3188.
122. Gopidas KR, et al. Photophysical and photochemical aspects of coupled semiconductors: charge-transfer processes in colloidal cadmium sulfide-titania and cadmium sulfide-silver (I) iodide systems. *J Phys Chem* 1990; 94: 6435-6440.
123. Nayak BB, et al. Structural characterization of Bi_{2-x}Sb_xS₃ films prepared by the dip-dry method. *Thin Solid Film* 1983; 105: 17-24.
124. Bessekhouad Y, et al. Bi₂S₃/TiO₂ and CdS/TiO₂ heterojunctions as an available configuration for photocatalytic degradation of organic pollutant. *J Photochem Photobiol A Chem* 2004; 163: 569-580.
125. Song KY, et al. Preparation of Transparent Particulate MoO₃/TiO₂ and WO₃/TiO₂ Films and Their Photocatalytic Properties. *Chem Mater* 2001; 13: 2349-2355.
126. Grandcolas M, et al. Porogen Template Assisted TiO₂ Rutile Coupled Nanomaterials for Improved Visible and Solar Light Photocatalytic Applications. *Catal Lett* 2008; 123: 65-71.
127. Wang C, et al. SnO₂ Nanostructures-TiO₂ Nanofibers Heterostructures: Controlled Fabrication and High Photocatalytic Properties. *Inorg Chem* 2009; 48: 7261-7268.
128. Vinodgopal K, et al. Nanostructured Semiconductor Films for Photocatalysis. Photoelectrochemical Behavior of SnO₂/TiO₂ Composite Systems and Its Role in Photocatalytic Degradation of a Textile Azo Dye. *Chem Mater* 1996; 8: 2180-2187.
129. Li X, et al. The synthesis of CdS/TiO₂ hetero-nanofibers with enhanced visible photocatalytic activity. *J Colloid Interface Sci* 2015; 452: 89-97.
130. Tamiolakis I, et al. Mesoporous CdS-sensitized TiO₂ nanoparticle assemblies with enhanced photocatalytic properties: Selective aerobic oxidation of benzyl alcohols. *Catal Today* 2015; 250: 180.
131. Doong RA, et al. The influence of pH and cadmium sulfide on the photocatalytic degradation of 2-chlorophenol in titanium dioxide suspensions. *Water Res* 2001; 35: 2873-2880.
132. Kang MG, et al. Enhanced photodecomposition of 4-chlorophenol in aqueous solution by deposition of CdS on TiO₂. *J Photochem Photobiol A* 1999; 125: 119-125.
133. Uddin Md T, et al. New Insights into the Photocatalytic Properties of RuO₂/TiO₂ Mesoporous Heterostructures for Hydrogen Production and Organic Pollutant Photodecomposition. *J Phys Chem C* 2015; 119: 7006-7015.
134. Wang H, et al. Semiconductor heterojunction photocatalysts: design, construction, and photocatalytic performance. *Chem Soc Rev* 2014; 43: 5234-5244.
135. Ai L, et al. Influence of substrate temperature on electrical and optical properties of p-type semitransparent conductive nickel oxide thin films deposited by radio frequency sputtering. *Appl Surf Sci* 2008; 254: 2401-2405.
136. Kokane SB, et al. Pd-TiO₂-SrIn₂O₄ heterojunction photocatalyst: enhanced photocatalytic activity for hydrogen generation and degradation of methylene blue. *RSC Adv* 2014; 4: 55539-55547.
137. Bickley RI, et al. A structural investigation of titanium dioxide photocatalysts. *J Solid State Chem* 1991; 92: 178-190.
138. Kho YK, et al. Photocatalytic H₂ Evolution over TiO₂ Nanoparticles. The Synergistic Effect of Anatase and Rutile. *J Phys Chem C* 2010; 114: 2821-2829.
139. Ohtani B, et al. What is Degussa (Evonik) P25? Crystalline composition analysis, reconstruction from isolated pure particles and photocatalytic activity test. *J PhotoChem Photobiol A: Chem* 2010; 216:179-182.
140. Su R, et al. How the Anatase-to-Rutile Ratio Influences the Photoreactivity of TiO₂. *Phys Chem C* 2011; 115: 24287-24292.
141. Verbruggen JJJ, et al. Surface photovoltage measurements: A quick assessment of the photocatalytic activity? *Catal Today* 2013; 209: 215-220.
142. Umabayashi T, et al. Band gap narrowing of titanium dioxide by sulfur doping. *Appl Phys Lett* 2002; 8: 454-456.

143. Mahmoodi NM and Arami MJ. Degradation and toxicity reduction of textile wastewater using immobilized titania nanophotocatalysis. *PhotoChem Photobiol B Biol* 2009; 94: 20-24.
144. Drioli E and Giorno L. *Comprehensive Membrane Science and Engineering*. Elsevier, Amsterdam, London 2010.
145. Pandey A, et al. Bacterial decolonization and degradation of azo dyes. *Int Biodeterior Biodegr* 2007; 59: 73-84.
146. Tunç S, et al. On-line spectrophotometric method for the determination of optimum operation parameters on the decolorization of Acid Red 66 and Direct Blue 71 from aqueous solution by Fenton process Original Research Article. *Chem Eng J* 2012; 181-182: 431-442.
147. Maurino V, et al. Polymer, particle, surfactant interactions. *Coll Surf A* 1999; 151: 329-338.
148. Tanaka K, et al. Photocatalytic Degradation of Commercial Azo Dyes. *Wat Res* 2000; 34: 327.
149. Daneshvar N, et al. Photocatalytic degradation of azo dye acid red 14 in water: investigation of the effect of operational parameters. *J PhotoChem Photobiol A: Chem* 2003; 157: 111-116.
150. Epling GA and Lin C. Photoassisted bleaching of dyes utilizing TiO₂ and visible light. *Chemosphere* 2002; 46: 561-570.
151. Liu Q, et al. Effect of factors on decolorization of azo dye Methyl orange by oxone/natural sunlight in aqueous solution. *Environ Sci Pollut Res* 2012; 19: 577-584.
152. Purkait MK, et al. Removal of Congo red using activated carbon and its regeneration. *J Hazard Mater* 2007; 145: 287-295.
153. Coleman R. The long-term contribution of dyes and stains to histology and histopathology. *Acta Histochemica* 2006; 108: 81-83.
154. Parwate DV, et al. Preliminary feasibility study of congo red dye as a secondary dosimeter. *Radiat Measurement* 2007; 42: 1527-1529.
155. Ljubas D, et al. Degradation of Methyl Orange and Congo Red dyes by using TiO₂ nanoparticles activated by the solar and the solar-like radiation. *J Environ Manage* 2015; 161: 83-91.
156. Kumar R, et al. Zero valent Ag deposited TiO₂ for the efficient photocatalysis of methylene blue under UV-C light irradiation. *Colloids Interf Sci Commun* 2015; 5: 1-4.
157. Khan MAN, et al. Removal of reactive blue 19 dye by sono, photo and sonophotocatalytic oxidation using visible light. *Ultrasonics Sonochem* 2015; 26: 370-377.
158. Dhatshanamurthi P, et al. Investigation on UV-A light photocatalytic degradation of an azo dye in the presence of CdO/TiO₂ coupled semiconductor. *Mater Sci Semiconductor Process* 2015; 35: 22-29.
159. Vaiano V, et al. Nanostructured N-doped TiO₂ coated on glass spheres for the photocatalytic removal of organic dyes under UV or visible light irradiation. *Appl Catal B* 2015; 170-171: 153-161.
160. Khanand H and Berk D. Characterization and mechanistic study of Mo⁺⁶ and V⁺⁵ codoped TiO₂ as a photocatalyst. *J Photochem Photobiol A: Chem* 2014; 294: 96-109.
161. Zhang J, et al. Synthesis and properties of (Yb, N)-TiO₂ photocatalyst for degradation of methylene blue (MB) under visible light irradiation. *Mater Res Bull* 2015; 70: 358-364.
162. Zhang W, et al. Effects of Al doping on properties of xAl-3%In-TiO₂ photocatalyst prepared by a sol-gel method. *Mater Sci Semiconductor Process* 2015; 38: 24-30.
163. Pal NK and Kryschi C. Improved photocatalytic activity of gold decorated differently doped TiO₂ nanoparticles: A comparative study. *Chemosphere* 2016; 144: 1655-1664.
164. Pol R, et al. Ni-, Pt- and (Ni/Pt)-doped TiO₂ nanophotocatalysts: A smart approach for sustainable degradation of Rhodamine B dye. *Appl Catal B: Envir* 2016; 181: 270-278.
165. Hoffmann MR, et al. Environmental Applications of Semicond Photocatalysis. *Chem Rev* 1995; 95: 69-96.
166. Zhang ML, et al. Novel preparation of nanosized ZnO-SnO₂ with high photocatalytic activity by homogeneous co-precipitation method. *Lett* 2005; 59: 3641-3644.
167. Sakthivel S, et al. Enhancement of photocatalytic activity by semiconductor heterojunctions: α-Fe₂O₃, WO₃ and CdS deposited on ZnO. *J PhotoChem Photobiol A* 2002; 148: 283-293.
168. Adán C, et al. Structure and activity of nanosized iron-doped anatase TiO₂ catalysts for phenol photocatalytic degradation. *Appl Catal B* 2007; 72: 11-17.
169. Lukáč J, et al. Influence of Zr as TiO₂ doping ion on photocatalytic degradation of 4-chlorophenol. *Appl Catal B* 2007; 74: 83-91.
170. Kuriakose S, et al. Visible light driven photocatalytic degradation of the reactive red-198, methylene blue and 3-chloro phenol by Nb₂O₅@Zno:Synthesis and characterization. *Adv Mater Lett* 2015; 6: 217-223.

171. Rez M, et al. Sensitivity analysis of the photoactivity of Cu-TiO₂/ZnO during advanced oxidation reaction by Adaptive Neuro-Fuzzy Selection Technique. *Measurement* 2016; 77: 155-174.
172. Herández-Alonso MD, et al. EPR study of the photoassisted formation of radicals on CeO₂ nanoparticles employed for toluene photooxidatio. *Appl Catal B* 2004; 50: 167-175.
173. Ji PF, et al. Ordered Mesoporous CeO₂ Synthesized by Nanocasting from Cubic Ia3d Mesoporous MCM-48 Silica: Formation, Characterization and Photocatalytic Activity. *J Phys Chem C* 2008; 112: 17809-17813.
174. Ji P, et al. Study of adsorption and degradation of acid orange 7 on the surface of CeO₂ under visible light irradiation. *Appl Catal B* 2009; 85: 148.
175. Zhai Y, et al. Preparation, characterization and photocatalytic activity of CeO₂ nanocrystalline using ammonium bicarbonate as precipitant. *Mater Lett* 2007; 61: 1863.
176. Hu KH, et al. Synthesis and photocatalytic properties of nano-MoS₂/kaolin composite. *Chem Eng J* 2010; 836-843.
177. Richardson JT. Electronic properties of unsupported cobalt-promoted molybdenum sulfide. *J Catal* 1988; 112: 313-319.
178. Ho WK, et al. Preparation and Photocatalytic Behavior of MoS₂ and WS₂ Nanocluster Sensitized TiO₂. *Langmuir* 2004; 20: 5865-5869.
179. Liu H, et al. Efficient synthesis of MoS₂ nanoparticles modified TiO₂ nanobelts with enhanced visible-light-driven photocatalytic activity. *J Mol Catal A: Chem* 2015; 396: 136-142.
180. Pan Z, et al. Photocatalytic degradation of 17 α -ethinylestradiol (EE2) in the presence of TiO₂-doped zeolite. *J Hazard Mater* 2014; 279: 17-25.
181. Todorova N, et al. Giannakopoulou T, Karapati S, Petridis D, Vaimakis T, and Trapalis C. Composite TiO₂/clays materials for photocatalytic NOx oxidation. *Appl Surf Sci* 2014; 319: 113-120.
182. Sangkhun W, et al. Photocatalytic degradation of BTEX using W-doped TiO₂ immobilized on fiberglass cloth under visible light. *Super lattice Microst* 2012; 52: 632-642.
183. Ye SY, et al. Photoelectrocatalytic decomposition of ethylene using TiO₂/activated carbon fiber electrode with applied pulsed direct current square-wave potential. *Appl Surf Sci* 2015; 341: 61-68.
184. Zhang P, et al. Magnetic recyclable TiO₂/multi-walled carbon nanotube nanocomposite: Synthesis, characterization and enhanced photocatalytic activity. *J Mol Catal A Chem* 2015; 402: 17-22.
185. Maraschi F, et al. TiO₂-modified zeolites for fluoroquinolones removal from wastewaters and reuse after solar light regeneration. *J Environ Chem Eng.* 2014; 2: 2170-2176.
186. Zhang W, et al. Fabrication of TiO₂/MoS₂@zeolite photocatalyst and its photocatalytic activity for degradation of methyl orange under visible light. *Appl Surf Sci* 2015; 358: 468-478.
187. Jiang Z, et al. A new visible light active multifunctional ternary composite based on TiO₂-In₂O₃ nanocrystals heterojunction decorated porous graphitic carbon nitride for photocatalytic treatment of hazardous pollutant and H₂ evolution. *Appl Catal B* 2015; 195: 170-171.
188. Sampaio MJ, et al. Carbon-based TiO₂ materials for the degradation of Microcystin-LA. *Appl Catal B* 2015; 170-171: 74.
189. Liu S, et al. Preparation of α -Fe₂O₃-TiO₂/fly ash cenospheres photocatalyst and its mechanism of photocatalytic degradation. *Colloids Surf A: PhysicoChem Eng Aspects* 2015; 484: 434-440.
190. Obregon S and Colón G. Heterostructured Er³⁺ doped BiVO₄ with exceptional photocatalytic performance by cooperative electronic and luminescence sensitization mechanism. *Appl Catal B Environ* 2013; 140-141: 242-249.
191. Lu Y, et al. Bi₂WO₆/TiO₂/Pt nanojunction system: A UV-vis light responsive photocatalyst with high photocatalytic performance. *Colloids Surf A: PhysicoChem Eng Aspects* 2015; 481: 252-260.
192. Xiong D, et al. Preparation and characterization of CuCrO₂/TiO₂ heterostructure photocatalyst with enhanced photocatalytic activity. *Appl Surf Sci* 2015; 347: 747-754.
193. Bhuyan D, et al. Magnetically recoverable Fe₃O₄@SBA-15: An improved catalyst for three component coupling reaction of aldehyde, amine and alkyne. *Catal Commun* 2015; 58: 158-163.
194. Xin T, et al. A facile approach for the synthesis of magnetic separable Fe₃O₄@TiO₂ core-shell nanocomposites as highly recyclable photocatalysts. *Appl Surf Sci* 2014; 288: 51-59.
195. Tezuka K, et al. Photocatalytic degradation of acetic acid on spinel ferrites MFe₂O₄ (M = Mg, Zn, and Cd). *Catal Comm* 2014; 48: 11-14.
196. ShihY-J, et al. Synthesis of magnetically recoverable ferrite (MFe₂O₄, M double bond; length as m-dash Co, Ni and Fe)-supported TiO₂ photocatalysts for decolorization of methylene blue. *Catal Comm* 2015; 72: 127-132.